Atmospheric
Chemistry
and Physics
Discussions

Open Access

Global and regional modeling of clouds and aerosols in the marine boundary layer during VOCALS: the VOCA Intercomparison

M. C. Wyant[1], C. S. Bretherton[1], R. Wood[1], G. R. Carmichael[2], A. Clarke[3], J. Fast[4], R. George[1], W. I. Gustafson Jr.[4], C. Hannay[5], A. Lauer[6,*], Y. Lin[7,**], J.-J. Morcrette[8], J. Mulcahy[9], P. E. Saide[2], S. N. Spak[2], and Q. Yang[4]

[1]Department of Atmospheric Sciences, University of Washington, Seattle, WA, USA
[2]Center for Global and Regional Environmental Research (CGRER), University of Iowa, Iowa City, IA, USA
[3]School of Ocean and Earth Science Technology (SOEST), University of Hawaii at Manoa, Honolulu, HI, USA
[4]Pacific Northwest National Laboratory, Richland, WA, USA
[5]National Center for Atmospheric Research, Boulder, CO, USA
[6]International Pacific Research Center, University of Hawaii at Manoa, Honolulu, HI
[7]Geophysical Fluid Dynamics Laboratory, Princeton, NJ, USA
[8]European Center for Medium-Range Forecasts, Shinfield Park, Reading, UK

ACPD

14, 6537–6587, 2014

Modeling of clouds and aerosols during VOCALS

M. C. Wyant et al.

Title Page

Abstract	Introduction
Conclusions	References
Tables	Figures

◄	►
◄	►
Back	Close

Full Screen / Esc

Printer-friendly Version

Interactive Discussion

[9]Met Office, Exeter, UK
[*]now at: Institute for Advanced Sustainability Studies, Potsdam, Germany
[**]now at: Ministry of Education Key Laboratory for Earth System Modeling, Center of Earth System Sciences, Tsinghua University, Beijing, China

Correspondence to: M. C. Wyant (mwyant@atmos.washington.edu)

Discussion Paper | Discussion Paper | Discussion Paper | Discussion Paper | Discussion Paper |

Title Page

Abstract	Introduction
Conclusions	References
Tables	Figures

|◄ | ►|

◄ | ►

| Back | Close |

Full Screen / Esc

Printer-friendly Version

Interactive Discussion

Modeling of clouds
and aerosols during
VOCALS

M. C. Wyant et al.

Title Page

Abstract | Introduction

Conclusions | References

Tables | Figures

◀◀ | ▶▶

◀ | ▶

Back | Close

Full Screen / Esc

Printer-friendly Version

Interactive Discussion

Abstract

A diverse collection of models are used to simulate the marine boundary layer in the Southeast Pacific region during the period of the October–November 2008 VOCALS REx field campaign. Regional models simulate the period continuously in boundary-forced free-running mode, while global forecast models and GCMs are run in forecast mode. The models are compared to extensive observations along a line at 20° S extending westward from the South American coast. Most of the models simulate cloud and aerosol characteristics and gradients across the region that are recognizably similar to observations, despite the complex interaction of processes involved in the problem, many of which are parameterized or poorly resolved. Some models simulate the regional low cloud cover well, though many models underestimate MBL depth near the coast. Most models qualitatively simulate the observed offshore gradients of SO_2, sulfate aerosol, CCN concentration in the MBL, and the related gradient in cloud droplet concentrations, but there are large quantitative intermodel differences in both means and gradients of these quantities. Most models underestimate large CCN (at 0.1 % supersaturation) in the MBL and free troposphere. The GCMs also have difficulty simulating coastal gradients in CCN and cloud droplet number concentration. The overall performance of the models demonstrates their potential utility in simulating aerosol-cloud interactions in the MBL, though quantitative estimation of aerosol-cloud interactions and aerosol indirect effects of MBL clouds with these models remains uncertain.

1 Introduction

The Southeast Pacific (SEP) region has an unusually extensive and persistent low-cloud cover supported by relatively low sea surface temperatures (SSTs) due to coastal upwelling, strong subsidence, and high static stability in the lower troposphere. There are typically strong east-west aerosol gradients in this marine boundary layer (MBL) between relatively pristine conditions in air masses advecting from the South Pacific

Ocean and more polluted air near the west coast of South America (e.g. Bretherton et al., 2010; Allen et al., 2011). Anthropogenic aerosol and aerosol precursor emissions from industrial, agricultural, and transportation sources are incorporated into the MBL directly or through intermittent free-tropospheric flow over the ocean and subsequent entrainment into the MBL (e.g. Clarke et al., 2010; George et al., 2013).

The persistent clouds and aerosol gradients make the SEP an attractive testbed for evaluating how well modern climate models can simulate aerosol-cloud interactions, a key uncertainty in understanding the 20th century climate record and an important issue for climate projection (IPCC 2007). This was a central motivation for the Variability of the American Monsoon Systems (VAMOS) Ocean–Cloud–Atmosphere–Land Study Regional Experiment (VOCALS-REx field campaign, which took place in the SEP region during October and November 2008 (Wood et al., 2011).

In addition to the features given above, many factors coincide to make the SEP unique in terms of its persistent cloud deck. The subsiding air above the MBL is also exceptionally dry, enhancing radiative cooling of the MBL clouds. The temperature inversion at the top of the MBL in the region is extremely strong, commonly exceeding 12 K during the austral spring. Another prominent feature influencing regional meteorology and climate is the Andes mountain range, which forms a long, mostly north-south barrier to east-west flow in the MBL (Richter and Mechoso, 2006). This feature together with the strong inversion controls the circulations that affect aerosol and chemical transport pathways. The meteorology of the region in the Austral spring season is dominated by a subtropical anticyclone. The flow in the MBL (Fig. 1) is typically southerly near the coast turning southeasterly away from the coast. There is a climatological advection of coastal air to the northwest, away from the coast and towards higher SSTs. The MBL deepens as it is advected offshore over higher SSTs. This flow pattern also carries aerosols from coastal anthropogenic and natural sources offshore. Aerosols generated farther inland and/or lofted upwards may also enter the SEP MBL through advection offshore at higher levels and entrainment into the MBL-top (Saide et al., 2012; George et al., 2013).

Skillful simulation of aerosol-cloud interaction in the MBL requires a realistic representation of other boundary layer cloud processes in models. However, the accurate simulation of boundary layer clouds such as stratocumulus and trade cumulus is a long-standing challenge in climate and forecast modeling. The Pre-VOCALS Assessment
5 (PreVOCA, Wyant et al., 2010) was designed to document and evaluate a wide range of models in the SEP region and to provide a benchmark for future model comparisons to VOCALS-REx observations. PreVOCA examined simulations of the VOCALS-REx study region for October 2006 using a collection of 15 regional and global models and compared them with satellite data and ship-based climatologies available before
10 VOCALS-REx. Most of these models had no representation of aerosol-cloud interactions. Many of the models produced serious biases in the time-mean geographic variability of low cloud in this region. In most models, the simulated MBL was too shallow near the coast. Nevertheless, a subset of models simulated the space-time distribution of cloud cover and thickness quite well.

15 The extensive in-situ sampling during VOCALS-REx, especially from aircraft, provides more detailed and direct comparisons for models than were available for Pre-VOCA. These include comparisons of aerosol and chemical constituents (Bretherton et al., 2010; Allen et al., 2011) as well as MBL vertical structure and precipitation. This dataset is uniquely suited to testing simulations of MBL cloud, aerosols, and their
20 interactions. The VOCALS Assessment (VOCA) was organized to capitalize on this opportunity.

Participating models simulated the SEP during the month of VOCALS-REx when aircraft observations were being made. Sixteen modeling groups submitted simulations from global climate models, global operational forecast models, and regional models.
25 In this study we focus on a subset of 9 VOCA models that have some representation of aerosols and their effects on clouds.

There are a number of prior modeling studies of the SEP during VOCALS REx. Abel et al. (2010) evaluate the simulations of cloud cover, MBL depth, and precipitation over the entire REx period as well as over the diurnal cycle using a limited area model

(LAM) configuration of the UK Met Office Unified Model. Yang et al. (2011) compare their WRF-Chem simulations for VOCA with observations and find that their simulations with interactive aerosols perform better than those with a passive treatment of aerosols. Their follow-up modeling study (Yang et al., 2012) quantified the relative impacts of regional anthropogenic and oceanic emissions on aerosol properties, cloud macro- and microphysics, and cloud radiative forcing over the SEP during VOCALS, and reported a large aerosol lifetime effect over the more susceptible clean ocean environment. Saide et al. (2012), using a different configuration of WRF-Chem, compare their VOCA simulations with observations over the entire study period as well as over shorter episodes. They also find that aerosol indirect effects play an important role in their simulations, and that their treatment of aerosol wet deposition has a strong impact on their results. George et al. (2013) use WRF-Chem in a similar configuration to their runs presented here to study multi-day "hook" events, where polluted continental air is carried offshore and influences stratocumulus clouds via aerosol indirect effects.

This paper addresses several questions: can the models represent the geographical contrasts in cloud microphysical properties in the SEP? What can the models tell us about the origins and impacts of aerosols in the region? How well do the models represent the impacts of these aerosols in the clouds? What problems are common to many models? Do these observations provide a good benchmark for aerosol/cloud interaction?

We will describe the setup of VOCA in Sect. 2. Section 3 compares the model results with each other and with observations. The results of the comparison will be discussed in Sect. 4 and conclusions presented in Sect. 5. Detailed descriptions of the models used are given in an Appendix.

2 Case setup

VOCA covers the time interval from 00:00 UTC 15 October 2008 through 00:00 UTC 16 November 2008, the period of VOCALS REx intensive airborne observations.

The outer study region for VOCA is shown in Fig. 1. The inner domain outlined in black extends from 12° S to 35° S and 68.5° W to 88° W, which includes the region of most of the REx research flights including the large set of flights along 20° S from the coast to 85° W. Simulation output data in the outer and inner region were horizontally averaged to a 1° × 1° grid and 0.25° × 0.25° grid, respectively, by the modeling groups. The models were not required to match their simulation domains to the outer and inner domains, or to necessarily include the outer study domain; the regional models in this comparison did not cover this outer study domain due to computational demands. Each model submitted data on its native vertical levels with 3 h time resolution, with some data fields averaged over 3 h intervals, and other fields provided at 3 h snapshots. The experiment specification can be found at http://www.atmos.washington.edu/~mwyant/vocals/model/VOCA_Model_Spec.htm.

A diverse group of models are represented in this study. They include global general circulation models (GCMs): the National Center for Atmospheric Research (NCAR) Community Atmosphere Model versions 4 and 5, (CAM4 and CAM5, respectively) and the NOAA Geophysical Fluid Dynamics Atmospheric Model 3 (GFDL AM3). Simulations using global weather forecast models were provided by the European Centre for Medium-Range Weather Forecasts (ECMWF) and the UK Met Office (UKMO). Regional simulations using the Weather Research and Forecasting model coupled with Chemistry (WRF-Chem) were submitted independently by research groups from University of Iowa, Pacific Northwest National Laboratory, and the University of Washington (hereafter labeled IOWA, PNNL, and UW, respectively). Another regional simulation included in this study was produced by the International Pacific Research Center (IPRC) with their Regional Atmospheric Model (iRAM). Detailed descriptions of these models are given in the Appendix.

Table 1 shows a list of the VOCA simulations analyzed in this study and many of their important parameters and characteristics. All of the listed global models were run in forecast mode, i.e., as a series of short simulations initialized at subsequent times from externally specified conditions. This initialization constrains the large-scale environ-

ment while still allowing the model to develop internally consistent representations of cloud and boundary layer structure. Forecast-mode has proven to be a good framework for identifying climate model biases (e.g. Phillips et al., 2004; Boyle et al., 2008; Hannay et al., 2009). Daily forecasts were provided by the modeling groups (twice-daily for the UKMO model), and for each model, data from these were stitched together to cover the REx period. The global weather forecast models used a data assimilation/forecast cycle that did not have a large initialization shock for boundary layer cloud, so the first forecast period (which presumably has the most accurate meteorological fields) was used in our study (e. g. 0–12 h for UKMO). The global climate models were initialized from ECMWF high-resolution global analyses produced for the Year of Tropical Convection (YOTC), so there was a spin up period for each model to adjust to this analysis. For such models, a later forecast period was chosen for analysis. The global models each utilize different land emission schemes.

All of the regional models were run continuously in free-running mode, with forcing at the lateral boundaries. The lateral boundary conditions for IOWA, UW, and iRAM came from the NCEP global FNL analysis, and for PNNL they came from NCEP's Global Forecast System (GFS) analyses. A regional emissions inventory of natural and man-made emissions over land during the VOCALS REx period was developed at University of Iowa. This inventory is described by Mena-Carrasco et al. (2012) and available at http://bio.cgrer.uiowa.edu/VOCA_emis/. It includes emissions from anthropogenic sources and large nearby volcanoes, but not biogenic or biomass burning emissions. All of the WRF-Chem regional models incorporated these emissions in their simulations, but none of the other participating models use these emissions. Parameterizations for fluxes of sea-salt and dimethyl sulfide (DMS) from the sea-surface were provided in the VOCA specification but not required for participants. The specified coarse and fine mode sea-salt emissions are based on Gong et al. (1997) and Monahan et al. (1986), while ultrafine emissions follow Clarke et al. (2006). The specification uses a simplified version of Nightingale et al. (2000) with a geographically uniform ocean surface DMS concentration of $2.8\,\text{nmol}\,\text{L}^{-1}$. Choice of emission param-

eterizations for any other aerosol types, such as dust, was left up to the participants. For regional models, the Model for Ozone and Related chemical Tracers version 4 (MOZART-4; Emmons et al., 2010) global model provided initial and lateral boundary conditions of aerosol and chemical species concentrations.

The models represent aerosol size and mass to varying degrees of precision and complexity. The IPRC model uses climatologically prescribed aerosol mass and size distributions and permits aerosols to affect clouds, and so surface aerosol emissions are not represented. The rest of the models use prognostic aerosol schemes – either they specify a small number of size modes (CAM5, GFDL, UW), or use sectional schemes with explicit aerosol size bins (PNNL, ECMWF, UKMO, IOWA). For models with aerosol-cloud feedbacks, a fraction of the aerosols can become activated and become cloud-droplet nuclei. In this way, aerosol number concentration can affect cloud-droplet number concentration (N_d). N_d in turn affects drizzle formation and cloud reflectivity. Cloud and precipitation scavenging reduces concentrations of both activated and unactivated aerosols in the MBL.

In this study, we rely heavily on in-situ aircraft observations along 20° S and between 70° W, at the Chilean coast, and 85° W, at the Improved Meteorology (IMET) moored research buoy situated about 1500 km offshore. Throughout VOCALS REx, several aircraft, primarily the NSF C-130 and UK BAe146, regularly performed research flights in and above the MBL along this line (Bretherton et al., 2010; Allen et al., 2011). A common flight pattern included a sequence of 60 km level legs, one 150–300 m above the inversion, one in the middle of the cloud layer or, in the absence of clouds, just below the inversion base, and one in the lower MBL at 150 m height. This pattern was repeated multiple times along the 20° S segment. Data from 23 flights are distributed fairly evenly throughout the 15 October to 16 November period and fairly evenly over the diurnal cycle. Almost all C-130 and BAe146 flights sampled out to 80° W, while 4 C-130 flights sampled the entire segment out to 85° W. Bretherton et al. (2010) and Allen et al. (2011) provided a thorough description of the flights and findings from this collection of flight data and other supporting observational data. Following those stud-

ies, we frequently sort aircraft leg-mean values into 5° or 2.5° longitude bins before further averaging in order to reduce sampling noise and facilitate comparisons with the models. The 25th and 75th percentile values of these leg-mean values are plotted in the figures as error bars and provide an estimate of the temporal and geographic variability in sampling. The actual measurement errors of the means should be much smaller than these ranges.

3   Results

3.1   Time-mean cloud macrophysics and precipitation

We begin by comparing simulated low-cloud fraction near 15:30 UTC (approximately 10.30 a.m. local time) averaged over the one-month REx period (Fig. 2) with satellite cloud fraction from the Moderate Resolution Imaging Spectrometer (MODIS) Terra daytime overpass (also approximately 10.30 a.m. local time). Note that the MODIS cloud fraction includes all clouds, not just low clouds, though low clouds strongly dominate the cloud fraction climatology. As in PreVOCA, many models have difficulty in simulating the geographic distribution of low-cloud fraction as compared with MODIS. The models' patterns of low-cloud cover are quite diverse. The PNNL, UW WRF, IOWA, and ECMWF models agree well with MODIS in the northeast part of the inner study region. In the southwest part of the region, PNNL and UW WRF have too little low cloud, while IOWA and ECMWF models have too much. In the southern half of the inner study region the CAM4 and CAM5, GFDL, UKMO, and IPRC models have too little low cloud in the southern part of the study region. While CAM5, with better vertical resolution, appears to be an improvement on CAM4 in the study region, the CAM5 low cloud fraction does not agree any better with MODIS than CAM4 in the outer region, despite better vertical resolution. The GFDL model also has too few low clouds near the coast. Along 20° S in the inner study region, the GFDL and UKMO models both significantly underestimate cloud fraction compared with MODIS.

Title Page

Abstract | Introduction

Conclusions | References

Tables | Figures

◄◄ | ►►

◄ | ►

Back | Close

Full Screen / Esc

Printer-friendly Version

Interactive Discussion

[CC BY]

Figure 3 compares the simulated liquid water path (LWP) along 20° S with mean C-130 airborne microwave radiometer observations (Zuidema et al., 2012) during VO-CALS and with mean satellite observations from the Advanced Microwave Scanning Radiometer-EOS (AMSR-E) on NASA's AQUA satellite. The AMSR-E values include both daytime and nighttime passes. Both satellite and aircraft measure a mean increase in LWP moving westward (offshore) from the near-coastal MBL and then a more constant LWP further offshore. The LWP of the models along 20° S varies considerably. Most of the models underpredict mean LWP over most of the 20° S profile, while a few models overpredict LWP nearer to the coast. Most models are a within a factor of two of the observed means.

Figure 4 shows the mean cloud-top height for all the models at 20° S compared with the mean of C-130 aircraft leg-mean cloud-top values. All of the models underestimate cloud-top height, with negative biases from 100 m to 700 m and particularly large biases near the coast. Similar underestimates of MBL depth near the coast were common in PreVOCA (Wyant et al., 2010). The WRF models compare better with aircraft observations than the other models along 20° S with negative biases less than 200 m in each longitude bin. The relative performance of various models is consistent with the study of Wang et al. (2011), which argues that both horizontal and vertical model resolution appear to be important in predicting MBL height. Most models match the observed westward increase of the cloud-top height. The main exception is the IPRC model in which cloud-top height rises too rapidly to the west, related to its strong negative bias in cloud-top height near the coast.

The general deepening of the boundary layer to the west along 20° S is also evident in Fig. 5, a comparison of the cloud fraction profiles at 75° W and 85° W. Also shown are profiles of cloud fraction from cloud-base and cloud-top measurements taken on *Ronald H. Brown* cruises during VOCALS REx along 20° S, which were sorted into measurements west of 80° W and east of 80° W (Burleyson et al., 2013). The periods of these measurements (25 October to 2 November 2008 and 10 November to 2 December 2008) only partly overlap with the VOCA study period. The modeled and

Modeling of clouds and aerosols during VOCALS

M. C. Wyant et al.

observed vertical extent of cloud fraction is broader to the west, consistent with a more decoupled vertical structure associated with cumuliform convection in the MBL and/or stronger time variations in inversion height. The overall distribution of modeled cloud heights is consistent with the cloud-top height comparison of Fig. 4. Models with fine vertical resolution in the MBL and lower troposphere (PNNL, IOWA) are able to represent the Gaussian shape of the measurements where models with coarser resolution show less smooth profiles. The height of peak cloud fraction in Fig. 5 is lower in almost all models than the corresponding observed peak, but in this case the comparison could be influenced by the mismatch of observation times and locations with those used for model averaging.

Mean surface precipitation rates in the region are generally very small, much less than $1 \, \mathrm{mm} \, \mathrm{day}^{-1}$ (Bretherton et al., 2010; Wood et al., 2012; Rapp et al., 2013), but precipitation processes still play an important role in the MBL. Drizzle redistributes moisture downward and stabilizes the MBL through evaporation. In this environment cloud and precipitation scavenging is the dominant removal process of sub-micron aerosols. Precipitation feedbacks also may play a central role in the formation and maintenance of pockets of open cells (POCs), which are common features of the regional marine stratocumulus (Bretherton et al., 2004; Wood et al., 2008, 2011; Ovchinnikov et al., 2013).

Figure 6 compares time-mean modeled surface precipitation, time-mean aircraft observations, and a 2006–2010 satellite precipitation climatology (Rapp et al., 2013) from the NASA CloudSat 2C-RAIN-PROFILE product that includes both daytime and nighttime passes. The aircraft measurements were made at about 150 m above the surface using the Particle Measuring Systems 2D-C instrument. Both observational datasets are subject to considerable uncertainty that is associated with both the measurement technique and the representativeness of the sampling. The models tend to produce more surface precipitation than suggested by CloudSat retrievals. Near the coast limited CloudSat observations suggest miniscule precipitation rates. Some models agree well with this (CAM5, UKMO, PNNL, and IOWA), while the other models predict more

I◄ | ►I

◄ | ►

Back | Close

Full Screen / Esc

significant precipitation rates. Offshore, all models are within an order of magnitude of observed values.

3.2 Time-mean aerosol and chemical properties

We next compare the simulated aerosol and chemical properties along 20° S with the REx observations. We focus on aerosols that directly impact MBL clouds in this region through their capacity to act as cloud condensation nuclei (CCN). We compare modeled and C-130 measured CCN number concentration at 0.1 % supersaturation in the free troposphere above the inversion (FT, Fig. 7, top-left panel) and at 150 m height (Fig. 7, bottom-left panel). The specification of 0.1 % supersaturation was in retrospect suboptimal for the intercomparison, since it is somewhat lower than the 0.2– 0.4 % maximum supersaturation expected during the nucleation of cloud droplets given typical MBL updraft strengths and aerosol size spectra (Martin et al., 1994; Snider et al., 2003; Hudson et al., 2010). This may lead to an underestimate of the actual number concentration of aerosol that nucleate cloud droplets. However, given other large parameterization uncertainties, this statistic is still a useful comparison between models and observations. In all figures, FT aircraft observations are sampled above cloud and between 1700 m and 3200 m, while model FT means are computed from the inversion height to 3200 m, following Allen et al. (2011). At 150 m, with the exception of the UKMO model, all of the models have mean CCN concentrations in the MBL and FT that are about half as large as observed or even less, both near shore and offshore. WRF-Chem models using the MOSAIC sectional aerosol scheme and the Abdul-Razzak and Ghan (2002) activation scheme (PNNL and IOWA) have significant concentrations of accumulation mode aerosol that do not activate at this low supersaturation, and aerosol concentrations show much better agreement with VOCALS observations in the MBL when these accumulation mode aerosols are considered (Yang et al., 2011; Saide et al., 2012). East of 80° W, the UKMO model has excessive CCN concentrations at all longitudes, reaching a peak of 1700 cm^{-3} at 74° W. In the FT the

Title Page

Abstract | Introduction

Conclusions | References

Tables | Figures

|◀ | ▶|

◀ | ▶

Back | Close

Full Screen / Esc

Printer-friendly Version

Interactive Discussion

model concentrations of the other models are also lower than observed. Most of the models have some semblance of the offshore CCN gradient seen in the observations.

Observational studies in the VOCALS region confirm that sulfate aerosol is the most important aerosol for nucleating cloud droplets (e.g. Twohy et al., 2013). While number concentration of accumulation-mode sulfate aerosol may be more directly relevant to cloud-aerosol interaction than sulfate mass, only the latter quantity was archived by most models and will be compared with observations. In the right panels of Fig. 7, modeled total mean sulfate aerosol mass is compared with C-130 and BAe-146 Aerosol Mass Spectrometer (AMS) sulfate aerosol mass from 0.05–0.5 μm. Here the model MBL values are vertical means with the MBL thickness determined as for Fig. 4. In both the MBL and the FT, the models all have significant offshore gradients of sulfate aerosol comparable to the observations, consistent with a continental source. The models differ considerably in sulfate mass, especially in the MBL, but the majority of models tend to have less FT and more MBL sulfate aerosol mass than the AMS values. It should be noted that the AMS values represent a lower bound on actual sulfate mass, as there can be significant mass contained in aerosols larger than 0.5 μm diameter (e.g. Yang et al., 2011). In the MBL, the models are more skillful representing sulfate mass than CCN number concentration, with most models within a factor of two of the observed means.

Two important atmospheric precursors to sulfate aerosol are dimethyl sulfide (DMS) and SO_2. DMS is the only local source of (non-sea-salt) sulfate aerosol in remote ocean regions. Figure 8 shows a comparison of mean MBL DMS concentration of most of the models. The concentrations are generally higher than observed, much higher for some models, and vary strongly between models. The specified ocean surface DMS concentration is a spatially uniform 2.8 nM for the WRF models (as given in the VOCA specification). While it may differ somewhat in the other models, the differences are very unlikely to account for the wide variation between models. Differences in mean surface wind speed and advection patterns also can not account for DMS differences. Over most of the inner study region, the interquartile range across models of mean model

surface wind speeds less than $2\,\mathrm{m\,s}^{-1}$ and the interquartile range of both meridional and zonal 10 m winds is less than $1.5\,\mathrm{m\,s}^{-1}$. Furthermore, the inter-model differences in upstream mean model wind speed appear to be uncorrelated with model mean DMS concentrations. The large differences in MBL DMS concentration are most likely due to differences in surface flux parameterizations or differences in model chemistry. Both models and observations agree that MBL DMS concentrations are larger offshore than near the coast, possibly due to the much higher wind speed offshore. PNNL WRF-Chem significantly overestimates the DMS concentration in the atmosphere, and detailed investigation by Yang et al. (2011) partially attributes this to overestimation of the DMS ocean-to-atmosphere transfer velocity. However, the PNNL WRF mean wind speeds along 20° S are very similar to UW WRF and GFDL, whose mean 20° S MBL DMS concentrations are much lower.

Both modeled and observed profiles of gas phase SO_2 along 20° S (Fig. 9) in the MBL and the FT show even sharper gradients near the coast than for SO_4 aerosol mass. There is abundant SO_2 near shore due to continental anthropogenic and natural sources, but the SO_2 is low offshore compared with aircraft values in both the MBL and the FT. The abundance of modeled SO_2 in the near shore and the strong modeled offshore sulfate gradient in the MBL suggests the models are producing most of their MBL sulfate aerosol east of 80° W via oxidation of SO_2. The offshore model differences in the FT SO_2 are likely due to differences in background SO_2 in the models. The only model that matches the observed values (IOWA) has specified minimum thresholds for its SO_2 boundary conditions (Saide et al., 2012). For the offshore MBL, most models, including the three WRF-Chem simulations, underestimate SO_2, which has been hypothesized to be due to SO_2 to SO_4 aqueous reaction rates that are too fast (Saide et al., 2012). However the aircraft concentrations in the remote MBL are suspiciously high, as there were almost no measured SO_2 concentrations below 10 pptv during VOCALS flights, even during nighttime.

Another significant potential source of aerosol mass and number in the MBL, especially in the remote regions, is sea-spray aerosol (SSA) generated by bubble bursting.

The SSA mass in the MBL is thought to be dominated by the largest 10 % of the total number concentration, with dry diameters exceeding 1 µm while number concentrations and contributions to CCN are dominated by the smaller sizes (Clarke et al., 2006). Here we compare modeled SSA (dry) mass mixing ratio with C-130 aircraft observed estimates (Fig. 10). These estimates from Blot et al. (2013) are based on data from particle counters and a Giant Nuclei Impactor and consider SSA particle sizes from about 0.04 µm to tens of micrometers. The observed trend to lower values west of 80° W has been attributed to more effective removal by drizzle in spite of higher winds and SSA production (Blot et al., 2013). There is a substantial range in simulated SSA mass, with most models exceeding the observed mean values. However, the WRF-Chem models and the GFDL models are generally close to the aircraft interquartile ranges. The inter-model range of mean surface wind speeds in the study region is small (as noted above) and uncorrelated with SSA mass. Some models have upper size limits due to the sectional approach used (e.g. the MOSIAC model used in the PNNL WRF and IOWA WRF has a 10 µm cutoff) limiting their total SSA mass somewhat. The expected mass contribution of aerosols smaller than 0.04 µm is negligible.

We next compare modeled cloud droplet number concentration, N_d with aircraft and MODIS observations (Fig. 11). Five of the seven plotted models underestimate droplet concentration compared with aircraft and MODIS observations, especially near the coast. (Note that model N_d is computed only in grid-cells where 3 h cloud liquid water exceeds $0.1\,g\,kg^{-1}$.) The general under-prediction of N_d is consistent with the under-prediction of the larger CCN by all models shown above. However, other model parameterizations, especially the representation of local updraft velocity and its role in droplet activation, can also play a large role in ultimately determining N_d. The majority of models do show the expected gradient in N_d moving away from the coast. The high UKMO concentrations near the coast are consistent with the extremely high CCN concentrations in that model. But the CAM5 and GFDL models have droplet concentrations near the coast that are not appreciably higher than farther offshore.

A strong connection between CCN and N_d in most models is evident in Figs. 12 and 13, which show their time evolution along 20° S over the duration of the experiment. CCN concentrations at 150 m are shown. Daily MODIS N_d from Bretherton et al. (2010) is also plotted during periods when local MODIS cloud fraction was greater

5 than 80 %, which are favorable for a reliable satellite-based N_d estimate. For some models, the LWC threshold for reporting simulated N_d often filters out results, especially during the early afternoon cloudiness minimum. Most models have higher CCN concentrations near the coast at most times, with occasional excursions of high CCN air westward coincident with periods of high N_d. The exceptions are the GFDL and the

10 IPRC models. The GFDL model has comparatively low liquid water concentrations, so N_d is unreported over much of the experiment domain and time making it difficult to discern N_d variations. IPRC has fixed aerosol concentrations which causes CCN concentrations to have minimal time dependence. The other models differ considerably in the westward extent and timing of high CCN and N_d excursions. Most models quali-

15 tatively agree about two periods of high CCN and N_d, also observed by MODIS, one from Julian Days (JD) 291–295, and one from JD315–320. The models tend to show two secondary peaks in CCN near JD302 and JD310, also visible in the MODIS N_d, but the temporal variation of modeled N_d during the middle of the study period is not consistent between models.

20 Black Carbon aerosol is a key tracer for the presence of sub-micrometer combustion derived aerosol. Although it is usually only a few percent of combustion aerosol mass, when BC is elevated above "clean" conditions it indicates combustion aerosol is contributing directly to aerosol mass, number and CCN. Unlike CO, BC in aged combustion aerosol is readily scavenged by precipitation such that ambient concentrations reflect

25 the impact of both source and removal processes. Figure 14 compares BC aerosol mass for several models with binned C-130 aircraft measurements made with a single particle soot photometer, which measures BC aerosol of diameter 0.087–0.4 μm (Shank et al., 2012). The models' spread in MBL concentrations is large, especially near the coast, but with all models generally within one order of magnitude of observed

Title Page

Abstract | Introduction

Conclusions | References

Tables | Figures

|◄ | ►|

◄ | ►

Back | Close

Full Screen / Esc

Printer-friendly Version

Interactive Discussion

means. Despite the large biases in many models, most do show an increase in black carbon concentration towards the coast in the MBL, as observed. One exception to this trend is UW. This model does not include biomass burning, which explains the large difference between it and the other models near land. The models generally underestimate BC in the FT. The FT observations are suggestive of an offshore maximum in BC that is not captured in any of the models. The spatial and temporal variability in aircraft measured BC in the FT makes evaluation of the model means difficult.

Two other trace gases measured during VOCALS flights are ozone and CO. Although they do not interact strongly with clouds, they provide an interesting comparison with models because this region is data-sparse and distant from other locations with extensive in-situ measurements through the lower troposphere. These gases (especially CO) are long lived; hence they are strongly determined by boundary conditions in the regional models. Thus these model comparisons, especially for CO, are a stronger test for global than regional models.

Ozone concentrations are compared in Fig. 15. As noted in Allen et al. (2011), mean O_3 concentrations measured in this region are higher in the free troposphere than in the MBL, generally consistent with subsidence of higher-ozone upper-tropospheric air, and the models reproduce this pattern. The PNNL WRF and IOWA WRF models match the observed means fairly well. Ozone can also be produced around anthropogenic pollution plumes. However, observed longitudinal gradients of O_3 are small in the boundary layer, and in the FT there actually is a 25 % drop in concentration near the coast; Allen et al. (2011) attributed this to enhanced mixing with ozone-poor boundary-layer air, which overwhelms any coastal anthropogenic source. The IOWA WRF and GFDL runs have a lesser but noticeable coastal decrease in O_3; the CAM models have a slight ozone increase in the MBL and no decrease in the FT, suggestive of an overly strong coastal ozone source.

CO concentrations (not shown) were available only from the WRF-Chem regional models and the GFDL global runs. Aircraft mean values from 75° W to 85° W were 66 ppbv in the MBL and 75 ppbv in the FT with weak longitudinal variation, and the

model means were generally within ±10 ppbv of observed means along 20° S in both the MBL and FT. Because of the relatively long lifetime of CO, differences between model means are more closely tied to model boundary conditions or remote sources than to differences in model physics and chemistry.

4   Discussion

In evaluating the performance of the models with respect to aerosols and clouds, it is useful to group a few subsets of the models with similar characteristics. We begin with two contemporary GCMs in the study, GFDL and CAM5, which have comparable horizontal and vertical resolution in the MBL. Both models significantly under predict LWP and inversion height along 20° S, and the GFDL model is significantly deficient in cloud fraction all along 20° S, especially near the coast. They also are both deficient in CCN at 0.1 % SS and have an apparent surplus of sulfate aerosol and SSA mass, suggesting that their aerosol size distributions may be skewed towards larger sizes. Neither model displays a mean offshore gradient in CCN despite having significant offshore gradients in sulfate aerosol. As a result both models underestimate observed cloud-droplet concentrations, especially near the coast.

The three participating WRF-Chem models (PNNL, IOWA, and UW) show somewhat differing cloud characteristics but are similar in some other respects. Since they use different PBL, microphysics, chemistry, and aerosol schemes, and use different horizontal and vertical grid resolutions, these models are expected to give a range of results. The three models produce similar geographic patterns of low cloud but the IOWA model predicts more low cloud in the southwest part of the study region than the other two models, while MODIS cloud fractions have intermediate values. Along 20° S, the PNNL model has the highest LWP while the IOWA and especially the UW model underpredict LWP away from the coast.

On the other hand, all three models only slightly underestimate the observed MBL depth. All three display prominent offshore gradients in CCN, N_d, and sulfate aerosol.

All three significantly underpredict CCN concentrations at 0.1 % supersaturation at 20° S. However the PNNL and IOWA models activate significantly more CCN at higher supersaturations (not shown). The UW and PNNL simulations only slightly underpredict N_d and the IOWA simulation is close to observations in the western part of
5 the study region but over predicts N_d in the eastern part.

The simulations from the two global operational forecast models, ECMWF and UKMO, contrast sharply. These models are intermediate in vertical resolution between the WRF models and the global climate models. The ECMWF LWP and cloud fraction agree reasonably well with observations though the MBL depth is shallower than
10 observed. The UKMO model maintains realistic MBL depth, but its low cloud fraction drops to 50–60 % away from the coast, somewhat less than observed, and the LWP is lower by a factor of two or more than observed. Because CCN concentration and N_d are unavailable from the ECMWF simulations, it is difficult to evaluate the ECMWF aerosol distribution. In contrast to other models in the study, UKMO has very high concentra-
15 tions of aerosol and CCN, leading to very large cloud droplet concentrations compared with those observed. The overestimation of sulphate aerosol was subsequently found to be due to a positive bias in the emission source strength used in these simulations introduced in error in the interpolation of the emissions onto the model grid.

Lastly, we compare salient aspects of model performance in VOCA to that in Pre-
20 VOCA by focusing on monthly-mean biases. A larger set of models, including many without aerosol physics, participated in VOCA as well as PreVOCA. In both intercomparisons, model simulation of surface pressure, lower tropospheric winds, and large-scale subsidence in the inner study region are in general agreement with each other and with reanalysis. In the VOCA models, the underestimate of MBL height near the
25 coast at 20° S tends to be slightly reduced. Mean distribution of low cloud in the region is still problematic and not substantively improved for many global models since PreVOCA, while regional models participating in both studies (IPRC and especially PNNL-WRF) exhibit better performance. Most models still tend to underestimate LWP

Modeling of clouds and aerosols during VOCALS

M. C. Wyant et al.

Title Page

Abstract | Introduction

Conclusions | References

Tables | Figures

◀ | ▶

◀ | ▶

Back | Close

Full Screen / Esc

Printer-friendly Version

Interactive Discussion

in the study region, especially GCMs with low vertical resolution, and the inter-model spread in LWP is still large.

5   Conclusions

Many models in this study are capable of qualitatively representing key aspects of aerosol processes in the MBL region, most notably the offshore gradient of SO_2, sulfate mass, CCN concentration and the related gradient in cloud droplet concentrations. Most models are within an order of magnitude of observations for most of these quantities. For some models, predicting cloud fraction remains a major challenge for simulating the climate of the SEP. Regional models perform better in this regard, and some have even improved their representation compared to the PreVOCA study. Most of the models in this study appear to be deficient in CCN at 0.1 % supersaturation both in the MBL and free troposphere. However, droplet number concentrations in many models are not far from observed values, indicating that for some models, significantly more accumulation mode aerosol is being activated than just the CCN at 0.1 % supersaturation. The GCMs in this study have difficulty with properly representing coastal gradients in CCN and cloud droplet number concentration near the coast. Low horizontal resolution may be to blame. There is also substantial scatter in model-predicted local sources of aerosol mass over the remote ocean due to DMS and SSA, even though the simulated wind speeds were realistic. While global models tend to have better DMS representation than regional models, the opposite occurs for SSA, where regional models show lower biases. The models show some skill in simulating the time-variation of aerosol and cloud droplet number concentrations associated with episodic offshore flow in the VOCALS study region.

The results suggest that although simulation of aerosol-cloud interactions and aerosol indirect effects of marine boundary layer clouds in these models is a challenge, and further improvements are needed, the models do capture many of the essential cloud and aerosol controlling processes in the SEP. Indeed, regional models are

already being successfully used to investigate aerosol processes in the SEP (e.g. Yang et al., 2011, 2012; Saide et al., 2012; George et al., 2013). Thorough integration of interactive aerosols into operational weather prediction models, a relatively new development, may help stimulate progress in this arena. To test the skill of future cloud-aerosol modeling systems, it will also be important to continue to evaluate them in detail with benchmark datasets such as the VOCALS REx observations, that comprehensively and simultaneously measure many of the relevant quantities.

Appendix A

Model descriptions

NCAR CAM4 and CAM5 are both part of the CESM1.0 release. The global NCAR CAM4 and CAM5 simulations were performed with similar setups with the finite volume dynamical core. Both use daily forecast runs initialized with ECMWF YOTC analyses interpolated onto the model grid, and are analyzed at hours 48–72. They use identical horizontal resolution, but with fewer vertical levels in CAM4, especially in the boundary layer. CAM4 uses a prognostic (liquid and ice) single moment microphysics scheme (Rasch and Kristjansson, 1998). CAM5 uses the two-moment prognostic bulk scheme including prognostic number concentration (Gettelman et al., 2008; Morrison and Gettelman, 2008). The PBL schemes also differ: CAM4 uses the non-local diffusivity scheme (Holtslag and Boville, 1993) while CAM5 uses the TKE based turbulence scheme of Bretherton and Park (2009) and the shallow convection scheme of Park and Bretherton (2009).

CAM4 is run here with a bulk aerosol scheme (MOZART, Lamarque et al., 2005 while CAM5 uses a prognostic aerosol model with three modes (MAM3). For sea-salt, CAM4 uses 4 bins, with sea-surface emission following Mahowald et al. (2006). CAM5 uses the sea-salt emission parameterization of Martensson et al. (2003). For SO_2 emissions CAM4 uses Smith et al. (2001) while CAM5 uses Smith et al. (2004).

For carbon emissions CAM4 uses Liousse et al. (1996) and Cooke et al. (1999), while CAM5 follows Bond et al. (2007) and Junker and Liousse (2008). For other land anthropogenic emissions, CAM5 uses the IPCC AR5 emissions (Lamarque et al., 2010). CAM4 uses a very similar radiation scheme to CAM 3 (Collins et al., 2006), while CAM5

5   uses the RRTMG scheme (Iacono et al., 2008) with a McICA approach. More detailed descriptions of CAM4 and CAM5 radiation, MAM3 and other physics can be found at http://www.cesm.ucar.edu/models/.

The IPRC model iRAM 1.2 is very similar to the version described in Lauer et al. (2009) but run at higher horizontal resolution ($0.25° \times 0.25°$). The simulations here

10   used NCEP Final Analysis (FNL) for initial and boundary conditions. Monthly mean aerosol concentrations are prescribed for these simulations based on global model simulations of aerosol mass (see Lauer et al., 2007) and observed aerosol size distributions (see McNaughton, 2008). Cloud microphysics are calculated with a two-moment bulk scheme (Phillips et al., 2007, 2008, 2009). Aerosol activation is tracked and af-

15   fects cloud microphysics, but cloud evolution and precipitation do not affect aerosol mass concentrations or sizes outside of clouds. The PBL scheme uses a turbulence closure with prognostic turbulent kinetic energy (TKE) and dissipation rate (Detering and Etling, 1985; Langland and Liou, 1996). The radiation scheme is based on Edwards and Slingo (1996).

20   The three WRF Chem simulations were run continuously over the study period and have similarly sized domains. UW and IOWA use NCEP FNL analyses and PNNL uses NCEP GFS analyses for initial and boundary conditions together with MOZART model output for initializing concentrations of chemical species and aerosols. All use the VOCA standard anthropogenic and volcanic land emissions. All use the RRTM

25   scheme (Mlawer et al., 1997) for LW radiation and the Goddard scheme (see Chou et al., 1998) for SW radiation. However the three simulations' horizontal and vertical resolutions differ, as do many of their other aerosol, cloud, and boundary layer physics parameterizations.

Modeling of clouds and aerosols during VOCALS

M. C. Wyant et al.

Title Page

Abstract   Introduction

Conclusions   References

Tables   Figures

|◄   ►|

◄   ►

Back   Close

Full Screen / Esc

Printer-friendly Version

Interactive Discussion

The IOWA run uses WRF Chem v3.3, and its configuration and physics are described in detail in Saide et al. (2012). The MOSAIC (Zaveri et al., 2008) 8-bin sectional aerosol scheme is used, with the CBM-Z gas-phase chemical mechanism (Zaveri and Peters, 1999) and modified DMS reactions. Biogenic land emissions are based on the MEGAN algorithm (Guenther et al., 2006) and biomass burning emissions are estimated from FIRMS MODIS fire detections (Davies et al., 2009). A bulk two-moment Lin microphysics scheme (see Chapman et al., 2009) and a level-2.5 Mellor-Yamada-type PBL scheme (MYNN 2.5, Nakanishi and Niino, 2004) are used.

The PNNL simulation uses modified WRF Chem v3.2.1 code, which was later released to the public in v3.3. The model is configured to use the MOSAIC 8-bin sectional aerosol module and the CBM-Z mechanism with DMS chemistry. The PNNL runs also use biogenic and biomass burning emissions from MEGAN and MODIS, respectively. The PNNL simulations differ in the use of the bulk two-moment microphysics scheme of Morrison (Morrison and Gettelman, 2008) and the YSU non-local PBL scheme (Hong et al., 2006). Additional details regarding the model's physical parameterizations and configuration for the PNNL simulations can be found in Yang et al. (2011 and 2012).

The UW contribution also uses WRF Chem v3.2.1, though on a coarser horizontal and vertical grid than the IOWA and PNNL runs. Aerosols are represented with 3 modes using the Modal Aerosol Dynamics Model for Europe (MADE, Ackerman et al., 1998) together with a Secondary Organic Aerosol Model (SORGAM, Schell et al., 2001). The Regional Acid Deposition Model, version 2 (RADM2) (Chang et al., 1989) chemical mechanism is used with modified DMS reactions. The UW run neglects biogenic and biomass burning emissions. For DMS flux, the UW run follows the VOCA specification. The same Lin microphysics scheme is used as the IOWA runs. Like CAM5, the TKE scheme of Bretherton and Park (2009) is used in the PBL but no shallow convection scheme is used.

The UKMO simulations use a deterministic global numerical weather prediction (NWP) configuration of the Met Office Unified Model (MetUM) (Davies et al., 2005) based on that in the Met Office's operational NWP suite between 9 March and 14

July 2010; this is designated global NWP cycle G52. Two main forecasts were run per day, each 5 days in length, initialized at 00:00 UTC and 12:00 UTC, for which the first 12 h are analyzed in this study. The Coupled Large-scale Aerosol Simulator for Studies in Climate (CLASSIC) prognostic aerosol scheme from the Met Office Hadley Centre was used (Bellouin et al., 2011). Aerosol concentrations are initialized from HadGEM-2 climatologies from a 20-year HadGEM2 climate run with the CLASSIC scheme. Aerosol emissions used are based on the AeroCom-2 hindcast emissions (Diehl et al., 2012) based on the year 2006. DMS emissions come from HadGEM2-based climatology. Local SSA over the ocean are diagnosed based on surface wind speed, and are not transported or deposited. Biogenic land aerosol is not modeled explicitly but instead comes from a climatology based on earlier simulations. A single moment bulk microphysics scheme (Wilson and Ballard, 1999), the Lock et al. (2000) PBL scheme, and the 2-stream radiation scheme of Edwards and Slingo (1996) were used.

The ECMWF runs use the Monitoring Atmospheric Composition and Climate (MACC) cycle model 36R1. Full model documentation is available at http://www.ecmwf.int/research/ifsdocs/CY33r1/index.html. Daily 24 h forecast runs are used with aerosols in the model as passive tracers. The model uses the aerosol scheme of Morcrette et al. (2009), which has 3 bins each for sea-salt and dust, single prognostic variables for SO_2 and SO_4, and 12 prognostic variables in all. The ECMWF model uses a bulk single-moment microphysics scheme. The RRTM radiation scheme is used with a McICA approach (Morcrette et al., 2008). The PBL in the model uses an eddy-diffusivity mass-flux framework (Köhler et al., 2011).

The GFDL AM3 (Donner et al., 2011) was run in forecast mode on a cubed-sphere $48 \times 48 \times 6$ grid with model output originally interpolated to a $2.0°$ latitude $\times 2.5°$ longitude grid. The runs were initialized with ECMWF reanalysis data. The GFDL modal aerosol scheme uses two modes for sulfate and organic aerosol, and three modes for sea salt (see Donner et al., 2011). Anthropogenic emissions are estimated from historical values of Lamarque et al. (2010). Biogenic emissions and DMS emissions from the ocean surface are also included. The microphysics scheme follows Rotstayn (1997) and Rot-

Modeling of clouds and aerosols during VOCALS

M. C. Wyant et al.

Title Page

Abstract	Introduction
Conclusions	References
Tables	Figures

|◀ | ▶|

| ◀ | ▶ |

| Back | Close |

Full Screen / Esc

Printer-friendly Version

Interactive Discussion

stayn et al. (2000) including prognostic cloud number concentration (Ming et al., 2006). The Lock et al. (2000) PBL scheme is used. The radiation scheme used is due to Freidenreich and Ramaswamy (1999) and Schwarzkopf and Ramaswamy (1999). See Donner et al. (2011) for more details.

References

Abdul-Razzak, H. and Ghan, S. J.: A parameterization of aerosol activation. 3. Sectional representation, J. Geophys. Res., 107, AAC 1-1–AAC 1-6, 2002.

20 Abel, S. J., Walters, D. N., and Allen, G.: Evaluation of stratocumulus cloud prediction in the Met Office forecast model during VOCALS-REx, Atmos. Chem. Phys., 10, 10541–10559, doi:10.5194/acp-10-10541-2010, 2010.

Ackermann, I. J., Hass, H., Memmesheimer, M., Ebel, A., Binkowski, F. S., and Shankar, U.: Modal aerosol dynamics model for Europe: development and first applications, Atmos. Environ., 32, 2981–2999, doi:10.1016/S1352-2310(98)00006-5, 1998.

25 Allen, G., Coe, H., Clarke, A., Bretherton, C., Wood, R., Abel, S. J., Barrett, P., Brown, P., George, R., Freitag, S., McNaughton, C., Howell, S., Shank, L., Kapustin, V., Brekhovskikh, V., Kleinman, L., Lee, Y.-N., Springston, S., Toniazzo, T., Krejci, R., Fochesatto, J., Shaw, G., Krecl, P., Brooks, B., McMeeking, G., Bower, K. N., Williams, P. I.,

Crosier, J., Crawford, I., Connolly, P., Allan, J. D., Covert, D., Bandy, A. R., Russell, L. M., Trembath, J., Bart, M., McQuaid, J. B., Wang, J., and Chand, D.: South East Pacific atmospheric composition and variability sampled along 20° S during VOCALS-REx, Atmos. Chem. Phys., 11, 5237–5262, doi:10.5194/acp-11-5237-2011, 2011.

5   Bellouin, N., Boucher, O., Haywood, J., Johnson, C., Jones, A., Rae, J., and Woodward, S.: Improved representation of aerosols for HadGEM2, Tech. Note 73, Hadley Cent. Met Office, Exeter, UK, 2007.

Bellouin, N., Rae, J., Jones, A., Johnson, C., Haywood, J., and Boucher., O.: Aerosol forcing in the Climate Model Intercomparison Project CMIP5 simulations by HadGEM2-ES and the role

10   of ammonium nitrate, J. Geophys. Res., 116, D20206, doi:10.1029/2011JD016074, 2011.

Blot, R., Clarke, A. D., Freitag, S., Kapustin, V., Howell, S. G., Jensen, J. B., Shank, L. M., McNaughton, C. S., and Brekhovskikh, V.: Ultrafine sea spray aerosol over the southeastern Pacific: open-ocean contributions to marine boundary layer CCN, Atmos. Chem. Phys., 13, 7263–7278, doi:10.5194/acp-13-7263-2013, 2013.

15   Bond, T. C., Bhardwaj, E., Dong, R., Jogani, R., Jung, S., Roden, C., Streets, D. G., and Trautmann, N. M.: Historical emissions of black and organic carbon aerosol from energy-related combustion, 1850–2000, Global Biogeochem. Cy., 21, GB2018, doi:10.1029/2006GB002840, 2007.

Boyle, J., Klein, S., Zhang, G., Xie, S., and Wei, X.: Climate model forecast experiments for

20   TOGA COARE, Mon. Weather Rev., 136, 808–832, doi:10.1175/2007MWR2145.1, 2008.

Bretherton, C. S. and Park, S.: A new moist turbulence parameterization in the Community Atmosphere Model, J. Climate, 22, 3422–3448, 2009.

Bretherton, C. S., Uttal, T., Fairall, C. W., Yuter, S., Weller, R., Baumgardner, D., Comstock, K., Wood, R., and Raga, G.: The EPIC 2001 stratocumulus study, B. Am. Meteorol. Soc., 85,

25   967–977, 2004.

Bretherton, C. S., Wood, R., George, R. C., Leon, D., Allen, G., and Zheng, X.: Southeast Pacific stratocumulus clouds, precipitation and boundary layer structure sampled along 20° S during VOCALS-REx, Atmos. Chem. Phys., 10, 10639–10654, doi:10.5194/acp-10-10639-2010, 2010.

30   Burleyson, C. D., de Szoeke, S. P., Yuter, S. E., Wilbanks, M., and Brewer, W. A.: Ship-based observations of the diurnal cycle of southeast Pacific marine stratocumulus clouds and precipitation, J. Atmos. Sci., 70, 3876–3894, doi:10.1175/JAS-D-13-01.1, 2013.

Chang, J. S., Binkowski, F. S., Seaman, N. L, McHenry, J. N, Samson, P. J., Stockwell, W. R., Walcek, C. J., Madronich, S., Middleton, P. B., Pleim, J. E., and Lansford, H. H.: The regional acid deposition model and engineering model, State-of-Science/Technology, Report 4, National Acid Precipitation Assessment Program, Washington D.C., 1989.

Chapman, E. G., Gustafson Jr., W. I., Easter, R. C., Barnard, J. C., Ghan, S. J., Pekour, M. S., and Fast, J. D.: Coupling aerosol-cloud-radiative processes in the WRF-Chem model: Investigating the radiative impact of elevated point sources, Atmos. Chem. Phys., 9, 945–964, doi:10.5194/acp-9-945-2009, 2009.

Chou, M. D., Suarez, M. J., Ho, C. H., Yan, M. M. H., and Lee, K. T.: Parameterizations for cloud overlapping and shortwave single-scattering properties for use in general circulation and cloud ensemble models, J. Climate, 11, 202–214, 1998.

Clarke, A. D., Owens, S. R., and Zhou, J.: An ultrafine sea-salt flux from breaking waves: implications for cloud condensation nuclei in the remote marine atmosphere, J. Geophys. Res., 111, D06202, doi:10.1029/2005JD006565, 2006.

Clarke, A. D., Freitag, S., Brekhovskikh, V., Campos, T., Snider, J. R., Kasputin, V., Howell, S., Shank, L., and McNaughton, C.: Combustion aerosol, entrainment, and clouds in the VO-CALS region, CLIVAR Exchanges, 15, 25–28, 2010.

Collins, W. D., Bitz, C. M., Blackmon, M. L., Bonan, G. B., Bretherton, C. S., Carton, J. A., Chang, P., Doney, S. C., Hack, J. J., Henderson, T. B., Kiehl, J. T., Large, W. G., McKenna, D. S., Santer, B. D., and Smith, R. D.: The community climate system model version 3 (CCSM3), J. Climate, 19, 2122–2143, 2006.

Cooke, W. F., Liousse, C., and Cachier, H.: Construction of a $1° \times 1°$ fossil fuel emission data set for carbonaceous aerosol and implementation and radiative impact in the ECHAM4 model, J. Geophys. Res., 104, 22137–22162, doi:10.1029/1999JD900187, 1999.

Davies, D. K., Ilavajahala, S., Wong, M. M., and Justice, C. O.: Fire Information for Resource Management System: archiving and distributing MODIS active fire data, IEEE T. Geosci. Remote, 47, 72–79, doi:10.1109/TGRS.2008.2002076, 2009.

Davies, T., Cullen, M. J. P., Malcolm, A. J., Mawson, M. H., Staniforth, A., White, A. A., and Wood, N.: A new dynamical core for the Met Office's global and regional modeling of the atmosphere, Q. J. Roy. Meteor. Soc., 131, 1759–1782, 2005.

Detering, H. W. and Etling, D.: Application of the E-ε turbulence model to the atmospheric boundary layer, Bound.-Lay. Meteorol., 33, 113–133, 1985.

Title Page

Abstract | Introduction

Conclusions | References

Tables | Figures

|◄ | ►|

◄ | ►

Back | Close

Full Screen / Esc

Printer-friendly Version

Interactive Discussion

Diehl, T., Heil, A., Chin, M., Pan, X., Streets, D., Schultz, M., and Kinne, S.: Anthropogenic, biomass burning, and volcanic emissions of black carbon, organic carbon, and SO_2 from 1980 to 2010 for hindcast model experiments, Atmos. Chem. Phys. Discuss., 12, 24895–24954, doi:10.5194/acpd-12-24895-2012, 2012.

Donner, L. J., Wyman, B. L., Hemler, R. S., and 38 co-authors: The dynamical core, physical parameterizations, and basic simulation characteristics of the atmospheric component AM3 of the GFDL Global Coupled Model CM3, J. Climate, 24, 3484–3519, 2011.

Edwards, J. M. and Slingo, A.: Studies with a flexible new radiation code. I: choosing a configuration for a large-scale model, Q. J. Roy. Meteor. Soc., 122, 689–719, 1996.

Emmons, L. K., Walters, S., Hess, P. G., Lamarque, J.-F., Pfister, G. G., Fillmore, D., Granier, C., Guenther, A., Kinnison, D., Laepple, T., Orlando, J., Tie, X., Tyndall, G., Wiedinmyer, C., Baughcum, S. L., and Kloster, S.: Description and evaluation of the Model for Ozone and Related chemical Tracers, version 4 (MOZART-4), Geosci. Model Dev., 3, 43–67, doi:10.5194/gmd-3-43-2010, 2010.

Freidenreich, S. M. and Ramaswamy, V.: A new multiple-band solar radiative parameterization for general circulation models, J. Geophys. Res., 104, 31389–31409, 1999.

George, R. C., Wood, R., Bretherton, C. S., and Painter, G.: Development and impact of hooks of high droplet concentration on remote southeast Pacific stratocumulus, Atmos. Chem. Phys., 13, 6305–6328, doi:10.5194/acp-13-6305-2013, 2013.

Gettelman, A., Morrison, H., and Ghan, S. J.: A new two-moment bulk stratiform cloud microphysics scheme in the Community Atmospheric Model, Version 3 (CAM3). Part II: Single-column and global results, J. Climate, 21, 3660–3679, 2008.

Gong, S. L., Barrie, L. A., and Blanchet, J.-P.: Modeling sea-salt aerosols in the atmosphere. 1. Model development, J. Geophys. Res., 102, 3805–3818, 1997.

Guenther, A., Karl, T., Harley, P., Wiedinmyer, C., Palmer, P. I., and Geron, C.: Estimates of global terrestrial isoprene emissions using MEGAN (Model of Emissions of Gases and Aerosols from Nature), Atmos. Chem. Phys., 6, 3181–3210, doi:10.5194/acp-6-3181-2006, 2006.

Hannay, C., Williamson, D. L., Hack, J. J., Kiehl, J. T., Olson, J. G., Klein, S. A., Bretherton, C. S., and Köhler, M.: Evaluation of forecasted Southeast Pacific stratocumulus in the NCAR, GFDL, and ECMWF models, J. Climate, 22, 2871–2889, doi:10.1175/2008JCLI2479.1, 2009.

6565

Holtslag, A. A. M. and Boville, B. A.: Local versus nonlocal boundary-layer diffusion in a global climate model, J. Climate, 6, 1825–1842, 1993.

Hong, S.-Y., Noh, Y., and Dudhia, J.: A new vertical diffusion package with an explicit treatment of entrainment processes, Mon. Weather Rev., 134, 2318–2341, 2006.

5   Hudson, J. G., Noble, S., and Jha, V.: Stratus cloud supersaturations, Geophys. Res. Lett., 37, L21813, doi:10.1029/2010GL045197, 2010.

Iacono, M. J., Delamere, J. S., Mlawer, E. J., Shephard, M. W., Clough, S. A., and Collins, W. D.: Radiative forcing by long-lived greenhouse gases: calculations with the AER radiative transfer models, J. Geophys. Res., 113, D13103, doi:10.1029/2008JD009944, 2008.

10 Junker, C. and Liousse, C.: A global emission inventory of carbonaceous aerosol from historic records of fossil fuel and biofuel consumption for the period 1860–1997, Atmos. Chem. Phys., 8, 1195–1207, doi:10.5194/acp-8-1195-2008, 2008.

Köhler, M., Ahlgrimm, M., and Beljaars, A.: Unified treatment of dry convective and stratocumulus-topped boundary layers in the ECMWF model, Q. J. Roy. Meteor. Soc., 137,

15 43–57, doi:10.1002/qj.713, 2011.

Lauer, A., Eyring, V., Hendricks, J., Jöckel, P., and Lohmann, U.: Global model simulations of the impact of ocean-going ships on aerosols, clouds, and the radiation budget, Atmos. Chem. Phys., 7, 5061–5079, doi:10.5194/acp-7-5061-2007, 2007.

Lauer, A., Wang, Y., Phillips, V. T. J., McNaughton, C. S., Bennartz, R., and Clarke, A. D.:

20 Simulating marine boundary layer clouds over the eastern Pacific in a regional climate model with double-moment cloud microphysics, J. Geophys. Res., 114, D21205, doi:10.1029/2009JD012201, 2009.

Lamarque, J.-F., Kiehl, J. T., Brasseur, G. P., Butler, T., Cameron-Smith, P., Collins, W. D., Collins, W. J., Granier, C., Hauglustaine, D., Hess, P. G., Holland, E. A., Horowitz, L.,

25 Lawrence, M. G., McKenna, D., Merilees, P., Prather, M. J., Rasch, P. J., Rotman, D., Shindell, D., and Thornton, P.: Assessing future nitrogen deposition and carbon cycle feedback using a multimodel approach: analysis of nitrogen deposition, J. Geophys. Res., 110, D19303, doi:10.1029/2005JD005825, 2005.

Lamarque, J.-F., Bond, T. C., Eyring, V., Granier, C., Heil, A., Klimont, Z., Lee, D., Liousse, C.,

30 Mieville, A., Owen, B., Schultz, M. G., Shindell, D., Smith, S. J., Stehfest, E., Van Aardenne, J., Cooper, O. R., Kainuma, M., Mahowald, N., McConnell, J. R., Naik, V., Riahi, K., and van Vuuren, D. P.: Historical (1850–2000) gridded anthropogenic and biomass burn-

ing emissions of reactive gases and aerosols: methodology and application, Atmos. Chem. Phys., 10, 7017–7039, doi:10.5194/acp-10-7017-2010, 2010.

Langland, R. H. and Liou, C.-S.: Implementation of an E-ε parameterization of vertical subgrid-scale mixing in a regional model, Mon. Weather Rev., 124, 905–918, 1996.

5 Liousse, C., Penner, J. E., Chuang, C., Walton, J. J., Eddleman, H., and Cachier, H.: A global three-dimensional model study of carbonaceous aerosols, J. Geophys. Res., 101, 19411–19432, doi:10.1029/95JD03426, 1996.

Lock, A. P., Brown, A. R., Bush, M. R., Martin, G. M., and Smith, R. N. B.: A new boundary layer mixing scheme. Part I: scheme description and single-column model tests, Mon. Weather

10 Rev., 128, 3187–3199, 2000.

Mahowald, N. M., Lamarque, J.-F., Tie, X. X., and Wolff, E.: Sea-salt aerosol response to climate change: last Glacial Maximum, preindustrial, and doubled carbon dioxide climates, J. Geophys. Res., 111, D05303, doi:10.1029/2005JD006459, 2006.

Mårtensson, E. M., Nilsson, E. D., de Leeuw, G., Cohen, L. H., and Hansson, H. C.: Laboratory

15 simulations are parameterization of the primary marine aerosol production, J. Geophys. Res., 108, 4297, doi:10.1029/2002JD002263, 2003.

Martin, G. M., Johnson, D. W., and Spice, A.: The measurement and parameterization of effective radius of droplets in warm stratocumulus clouds, J. Atmos. Sci., 51, 1823–1842, 1994.

McNaughton, C. S.: Constraining climate model simulations of aerosol size distributions over

20 the North Pacific and North America using in-situ airborne measurements, Ph.D. thesis, Univ. of Hawaii at Manoa, Honolulu, Hawaii, USA, 2008.

Mechoso, R., Wood, R., Bretherton, C. S., Weller, R., Clarke, A. D., Garreaud, R., Grados, C., McWilliams, J., de Szoeke, S., Yuter, S. E., Farrar, J. T., Feingold, G., Zuidema, P., Wilbanks, M., Chaigneau, A., and Echevin, A.: The coupled climate system of the Southeast

25 Pacific, B. Am. Meteorol. Soc., doi:10.1175/BAMS-D-11-00246.1, accepted, 2013.

Mena-Carrasco, M., Oliva, E., Saide, P., Spak, S. N., de la Maza, C., Osses, M., Tolvett, S., Campbell, J. E., Tsao, T. C.-C., and Molina, L. T.: Estimating the health benefits from natural gas use in transport and heating in Santiago, Chile, Sci. Total Environ., 429, 257–265, doi:10.1016/j.scitotenv.2012.04.037, 2012.

30 Ming, Y., V. Ramaswamy, V., Donner, L. J., and Phillips, V. T. J.: A new parameterization of cloud droplet activation applicable to general circulation models, J. Atmos. Sci., 63, 1348–1356, 2006.

Discussion Paper | Discussion Paper | Discussion Paper | Discussion Paper | Discussion Paper

Mlawer, E. J., Taubman, S. J., Brown, P. D., Iacono, M. J., and Clough, S. A.: Radiative transfer for inhomogeneous atmospheres: RRTM, a validated correlated-k model for the longwave, J. Geophys. Res., 102, 16663–16682, 1997.

Monahan, E. C., Spiel, D. E., and Davidson, K. L.: A model of marine aerosol generation via whitecaps and wave disruption, in: Oceanic Whitecaps and Their Role in Air-Sea Exchange Processes, edited by: Monahan, E. C. and Mac Niocaill, G., Springer, New York, 167–193, 1986.

Morcrette, J.-J., Barker, H. W., Cole, J. N. S., Iacono, M. J., and Pincus, R.: Impact of a new radiation package, McRad, in the ECMWF Integrated Forecasting System, Mon. Weather Rev., 136, 4773–4798, doi:10.1175/2008MWR2363.1, 2008.

Morcrette, J.-J., Boucher, O., Jones, L., Salmond, D., Bechtold, P., Beljaars, A., Benedetti, A., Bonet, A., Kaiser, J. W., Razinger, M., Schulz, M., Serrar, S., Simmons, A. J., Sofiev, M., Suttie, M., Tompkins, A. M., Untch, A.: Aerosol analysis and forecast in the ECMWF Integrated Forecast System: forward modelling, J. Geophys. Res., 114, D06206, doi:10.1029/2008JD011235, 2009.

Morrison, H. and Gettelman, A.: A new two-moment bulk stratiform cloud microphysics scheme in the Community Atmosphere Model, version 3 (CAM3). Part I: description and numerical tests, J. Climate, 21, 3642–3659, 2008.

Nakanishi, M. and Niino, H.: An improved Mellor-Yamada level-3 model with condensation physics: its design and verification, Bound.-Lay. Meteorol., 112, 1–31, 2004.

Nightingale, P. D., Malin, G., Law, C. S., Watson, A. J., Liss, P. S., Liddicoat, M. I., Boutin, J., and Upstill-Goddard, R. C.: In situ evaluation of air–sea gas exchange parameterizations using novel conservative and volatile tracers, Global Biogeochem. Cy., 14, 373–387, 2000.

Ovchinnikov, M., Easter, R. C., and Gustafson, W. I.: Untangling dynamical and micro-physical controls for the structure of stratocumulus, Geophys. Res. Lett., 40, 4432–4436, doi:10.1002/grl.50810, 2013.

Park, S. and Bretherton, C. S.: The University of Washington shallow convection and moist turbulence schemes and their impact on climate simulations with the community atmosphere model, J. Climate, 22, 3449–3469, 2009.

Phillips, T. J., Potter, G. L., Williamson, D. L., Cederwall, R. T., Boyle, J. S., Fiorino, M., Hnilo, J. J., Olson, J. G., Xie, S., and Yio, J. J.: Evaluating parameterizations in general circulation models: climate simulation meets weather prediction, B. Am. Meteorol. Soc., 85, 1903–1915, doi:10.1175/BAMS-85-12-1903, 2004.

Title Page

Abstract | Introduction

Conclusions | References

Tables | Figures

|◀ | ▶|

◀ | ▶

Back | Close

Full Screen / Esc

Printer-friendly Version

Interactive Discussion

Phillips, V. T. J., Donner, L. J., and Garner, S. T.: Nucleation processes in deep convection simulated by a cloud-system-resolving model with double-moment bulk microphysics, J. Atmos. Sci., 64, 738–761, doi:10.1175/JAS3869.1, 2007.

Phillips, V. T. J., DeMott, P. J., and Andronache, C.: An empirical parameterization of heterogeneous ice nucleation for multiple chemical species of aerosol, J. Atmos. Sci., 65, 2757–2783, doi:10.1175/2007JAAS2546.1, 2008.

Phillips, V. T. J., Andronache, C., Christner, B., Morris, C. E., Sands, D. C., Bansemer, A., Lauer, A., McNaughton, C., and Seman, C.: Potential impacts from biological aerosols on ensembles of continental clouds simulated numerically, Biogeosciences, 6, 987–1014, doi:10.5194/bg-6-987-2009, 2009.

Rapp, A. D., Lebsock, M., and L'Ecuyer, T.: Low cloud precipitation climatology in the southeastern Pacific marine stratocumulus region using CloudSat, Environ. Res. Lett., 8, 014027, doi:10.1088/1748-9326/8/1/014027, 2013.

Rasch, P. J. and Kristjánsson, J. E.: A comparison of the CCM3 model climate using diagnosed and predicted condensate parameterizations, J. Climate, 11, 1587–1614, 1998.

Richter, I. and Mechoso, C. R.: Orographic influences on subtropical stratocumulus, J. Atmos. Sci., 63, 2585–2601, 2006.

Rotstayn, L. D.: A physically based scheme for the treatment of stratiform clouds and precipitation in large-scale models. I: Description and evaluation of the microphysical processes, Q. J. Roy. Met. Soc., 123, 1227–1282, 1997.

Rotstayn, L. D.: On the "tuning" of autoconversion parameterizations in climate models, J. Geophys. Res., 105, 15495–15507, 2000.

Saide, P. E., Spak, S. N., Carmichael, G. R., Mena-Carrasco, M. A., Yang, Q., Howell, S., Leon, D. C., Snider, J. R., Bandy, A. R., Collett, J. L., Benedict, K. B., de Szoeke, S. P., Hawkins, L. N., Allen, G., Crawford, I., Crosier, J., and Springston, S. R.: Evaluating WRF-Chem aerosol indirect effects in Southeast Pacific marine stratocumulus during VOCALS-REx, Atmos. Chem. Phys., 12, 3045–3064, doi:10.5194/acp-12-3045-2012, 2012.

Schell, B., Ackermann, I. J., Hass, H., Binkowski, F. S., and Ebel, A.: Modeling the formation of secondary organic aerosol within a comprehensive air quality model system, J. Geophys. Res., 106, 28275–28293, 2001.

Schwarzkopf, M. D. and Ramaswamy, V.: Radiative effects of CH_4, N_2O, halocarbons, and the foreign-broadened H_2O continuum: a GCM experiment, J. Geophys., Res., 104, 9467–9488, 1999.

Shank, L. M., Howell, S., Clarke, A. D., Freitag, S., Brekhovskikh, V., Kapustin, V., Mc-Naughton, C., Campos, T., and Wood, R.: Organic matter and non-refractory aerosol over the remote Southeast Pacific: oceanic and combustion sources, Atmos. Chem. Phys., 12, 557–576, doi:10.5194/acp-12-557-2012, 2012.

Smith., S. J., Pitcher, H., and Wigley, T. M. L.: Global and regional anthropogenic sulfur dioxide emissions, Global Biogeochem. Cy., 29, 99–119, 2001.

Smith, S. J., Andres, R., Conception, E., and Lurz, J.: Historical sulfur dioxide emissions 1850–2000: methods and results, Technical report, Pacific Northwest National Laboratory, Joint Global Change Research Institute, College Park, Maryland, USA, 2004.

Snider, J. R., Guibert, S., Brenguier, J.-L., and Putaud, J.-P.: Aerosol activation in marine stratocumulus clouds: 2. Köhler and parcel theory closure studies, J. Geophys. Res., 108, 8629, doi:10.1029/2002JD002692, 2003.

Twohy, C. H., Anderson, J. R., Toohey, D. W., Andrejczuk, M., Adams, A., Lytle, M., George, R. C., Wood, R., Saide, P., Spak, S., Zuidema, P., and Leon, D.: Impacts of aerosol particles on the microphysical and radiative properties of stratocumulus clouds over the southeast Pacific Ocean, Atmos. Chem. Phys., 13, 2541–2562, doi:10.5194/acp-13-2541-2013, 2013.

Wang, S., O'Neill, L. W., Jiang, Q., de Szoeke, S. P., Hong, X., Jin, H., Thompson, W. T., and Zheng, X.: A regional real-time forecast of marine boundary layers during VOCALS-REx, Atmos. Chem. Phys., 11, 421–437, doi:10.5194/acp-11-421-2011, 2011.

Wilson, D. R. and Ballard, S. P.: A microphysically based precipitation scheme for the UK Meteorological Office Unified Model, Q. J. Roy. Meteorol. Soc., 125, 1607–1636, 1999.

Wood, R., Comstock, K. K., Bretherton, C. S., Cornish, C., Tomlinson, J., Collins, D. R., and Fairall, C.: Open cellular structure in marine stratocumulus cloud sheets, J. Geophys. Res., 113, D12207, doi:10.1029/2007JD009371, 2008.

Wood, R., Bretherton, C. S., Leon, D., Clarke, A. D., Zuidema, P., Allen, G., and Coe, H.: An aircraft case study of the spatial transition from closed to open mesoscale cellular convection over the Southeast Pacific, Atmos. Chem. Phys., 11, 2341–2370, doi:10.5194/acp-11-2341-2011, 2011.

Wood, R., Mechoso, C. R., Bretherton, C. S., Weller, R. A., Huebert, B., Straneo, F., Albrecht, B. A., Coe, H., Allen, G., Vaughan, G., Daum, P., Fairall, C., Chand, D., Gallardo Klenner, L., Garreaud, R., Grados, C., Covert, D. S., Bates, T. S., Krejci, R., Russell, L. M., de Szoeke, S., Brewer, A., Yuter, S. E., Springston, S. R., Chaigneau, A., Toniazzo, T., Min-

nis, P., Palikonda, R., Abel, S. J., Brown, W. O. J., Williams, S., Fochesatto, J., Brioude, J., and Bower, K. N.: The VAMOS Ocean-Cloud-Atmosphere-Land Study Regional Experiment (VOCALS-REx): goals, platforms, and field operations, Atmos. Chem. Phys., 11, 627–654, doi:10.5194/acp-11-627-2011, 2011.

5 Wood, R., Leon, D., Lebsock, M., Snider, J., and Clarke, A. D.: Precipitation driving of droplet concentration variability in marine low clouds, J. Geophys. Res., 117, D19210, doi:10.1029/2012JD018305, 2012.

Wyant, M. C., Wood, R., Bretherton, C. S., Mechoso, C. R., Bacmeister, J., Balmaseda, M. A., Barrett, B., Codron, F., Earnshaw, P., Fast, J., Hannay, C., Kaiser, J. W., Kitagawa, H.,

10 Klein, S. A., Köhler, M., Manganello, J., Pan, H.-L., Sun, F., Wang, S., and Wang, Y.: The Pre-VOCA experiment: modeling the lower troposphere in the Southeast Pacific, Atmos. Chem. Phys., 10, 4757–4774, doi:10.5194/acp-10-4757-2010, 2010.

Yang, Q., W. I. Gustafson Jr., Fast, J. D., Wang, H., Easter, R. C., Morrison, H., Lee, Y.-N., Chapman, E. G., Spak, S. N., and Mena-Carrasco, M. A.: Assessing regional scale pre-

15 dictions of aerosols, marine stratocumulus, and their interactions during VOCALS-REx using WRF-Chem, Atmos. Chem. Phys., 11, 11951–11975, doi:10.5194/acp-11-11951-2011, 2011.

Yang, Q., Gustafson Jr., W. I., Fast, J. D., Wang, H., Easter, R. C., Wang, M., Ghan, S. J., Berg, L. K., Leung, L. R., and Morrison, H.: Impact of natural and anthropogenic aerosols

20 on stratocumulus and precipitation in the Southeast Pacific: a regional modelling study using WRF-Chem, Atmos. Chem. Phys., 12, 8777–8796, doi:10.5194/acp-12-8777-2012, 2012.

Zaveri, R. A. and Peters, L. K.: A new lumped structure photochemical mechanism for large-scale applications, J. Geophys. Res., 104, 30387–30415, 1999.

Zaveri, R. A., Easter, R. C., Fast, J. D., Peters, L.: Model for simulating aerosol interactions and

25 chemistry (MOSAIC), J. Geophys. Res., 113, D13204, doi:10.1029/2007JD008782, 2008.

Zuidema, P., Leon, D., Pazmany, A., and Cadeddu, M.: Aircraft millimeter-wave passive sensing of cloud liquid water and water vapor during VOCALS-REx, Atmos. Chem. Phys., 12, 355–369, doi:10.5194/acp-12-355-2012, 2012.

Title Page

Abstract | Introduction

Conclusions | References

Tables | Figures

I◄ | ►I

◄ | ►

Back | Close

Full Screen / Esc

Printer-friendly Version

Interactive Discussion

Table 1. Model parameters and physics.

| Model	Domain Extent	Horizontal Resolution, inner region (lat × lon)	Vertical Levels (> 700 hPa)	Forecast Frequency	Forecast Hours Analyzed	Aerosol Scheme	PBL Scheme	Land Emissions	Micro-physics	Aerosol–Cloud feedback	Investigators
CAM4	Global	1.9° × 2.5°	26 (6)	Daily	48–72	MOZART bulk (Lamarque et al., 2005)	Holtslag Boville (1993)	see Appendix	1-moment	no	C. Hannay
CAM5	Global	1.9° × 2.5°	30 (10)	Daily	48–72	MAM 3 modes	UW PBL	Lamarque et al. (2010)	2-moment Morrison	yes	C. Hannay
GFDL AM3	Global	2.0° × 2.5°	48 (12)	Daily	24–48	2 or 3 modes (Donner et al., 2010)	Lock et al. (2000)	Lamarque et al. (2010)	1-moment Rotstayn	yes	Y. Lin
ECMWF/MACC 36R1	Global	0.225° × 0.225°	91 (21)	Daily	0–24	sectional 8 bins Morrcette (2009)	eddy-diff mass-flux (Köhler et al., 2011)	Morcette et al. (2009)	1-moment bulk	No	J.-J. Morcette
UKMO MetUM, PS23, UM7.5	Global	0.375° × 0.562°	70 (20)	Twice Daily	0–12	CLASSIC Bellouin et al. (2007) sectional	Lock et al. (2000)	AeroCom-2	1-moment Wilson and Ballard	yes	J. Mulcahy
IPRC iRAM 1.2	170–40° W 40° S-40° N	0.25° × 0.25°	28 (12)	N/A	N/A	Prescribed	E-ε turbulence closure	N/A	2-moment Philipps	Aerosols affect clouds	A. Lauer Y. Wang
PNNL WRF-Chem 3.2.1	93–63° W 36–11° S	9km × 9km	64 (48)	N/A	N/A	MOSAIC sectional 8 bins	YSU PBL	VOCA specified	2-moment Morrison	yes	Q. Yang W.I. Gustafson J. D. Fast
IOWA WRF-Chem 3.3	91–65° W 40–12° S	12km × 12km	74 (53)	N/A	N/A	MOSAIC sectional 8 bins	MYNN 2.5	VOCA specified	2-moment Lin	yes	P. Saide
UW WRF-Chem 3.2.1	93–64° W 40–7° S	0.25° × 0.25°	27 (15)	N/A	N/A	MADE/SORGAM 3 modes	UW PBL	VOCA specified	2-moment Lin	yes	R. George R. Wood

SST
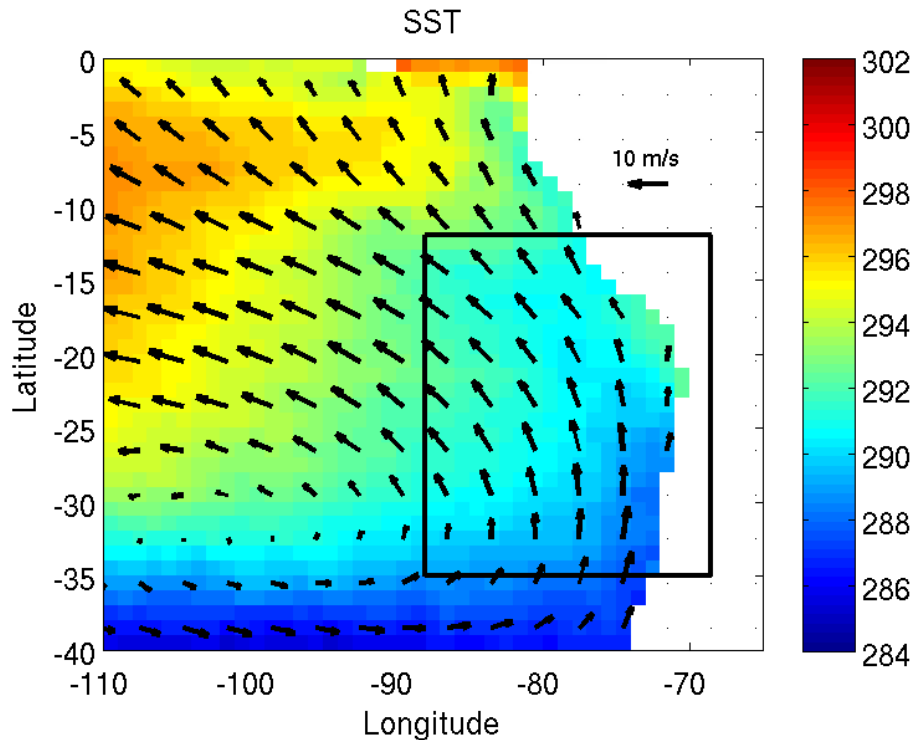
Fig. 1. Observed SST (K) from AMSR-E and surface winds from QuikSCAT in the outer VOCA study region during the REx period, 15 October–16 November 2008. The inner study region is shown as a black rectangle.
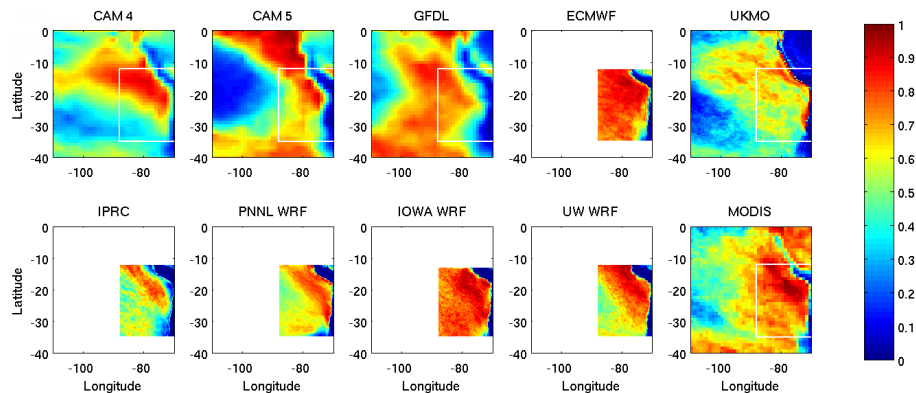
Fig. 2. Models' mean low cloud fraction at 10.30 a.m. local time (15:30 UTC) compared with MODIS Terra daytime mean total cloud fraction. The extent of the inner VOCA study region is shown with a white rectangle.
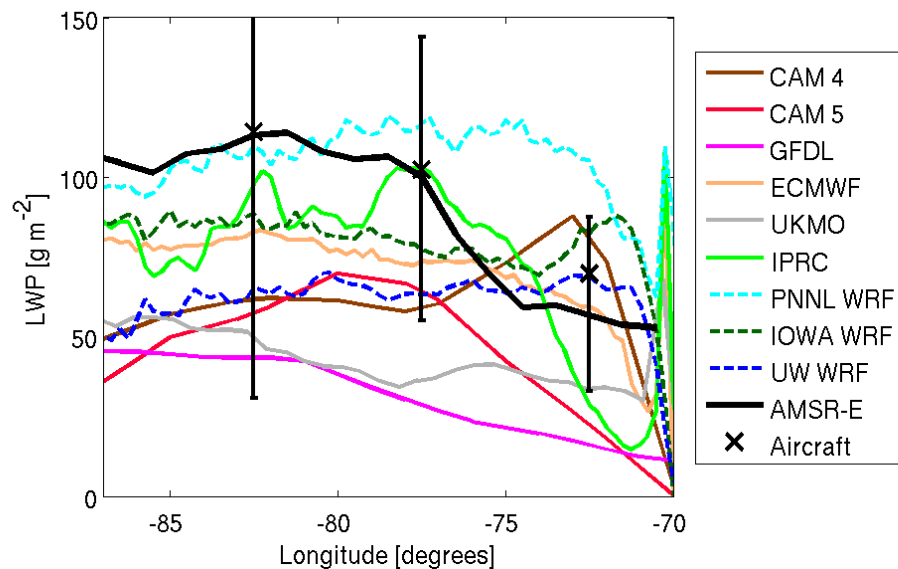
Fig. 3. Grid-box mean liquid water path (LWP) along 20° S compared with AMSR-E satellite mean and median LWP from microwave radiometer on the C-130 (Zuidema et al., 2012). Error bars represent interquartile ranges of aircraft leg-means.

Discussion Paper | Discussion Paper | Discussion Paper | Discussion Paper

ACPD

14, 6537–6587, 2014

Modeling of clouds and aerosols during VOCALS

M. C. Wyant et al.

Title Page

Abstract | Introduction

Conclusions | References

Tables | Figures

◄ | ►

◄ | ►

Back | Close

Full Screen / Esc

Printer-friendly Version

Interactive Discussion
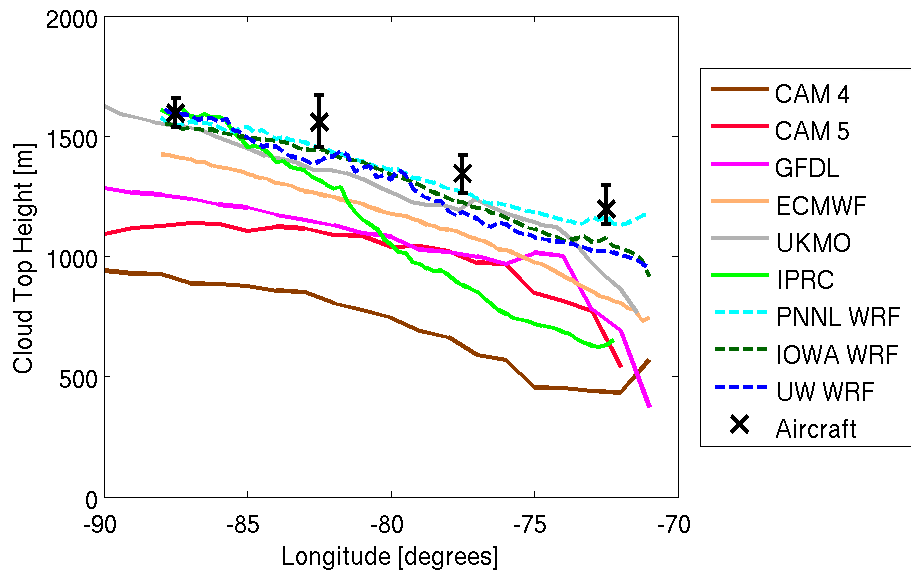
Fig. 4. Model-mean cloud-top height along 20° S compared with mean cloud-top measured using cloud radar from C-130 flights (Bretherton et al., 2010).

Title Page

Abstract | Introduction

Conclusions | References

Tables | Figures

I◄ | ►I

◄ | ►

Back | Close

Full Screen / Esc

Printer-friendly Version

Interactive Discussion
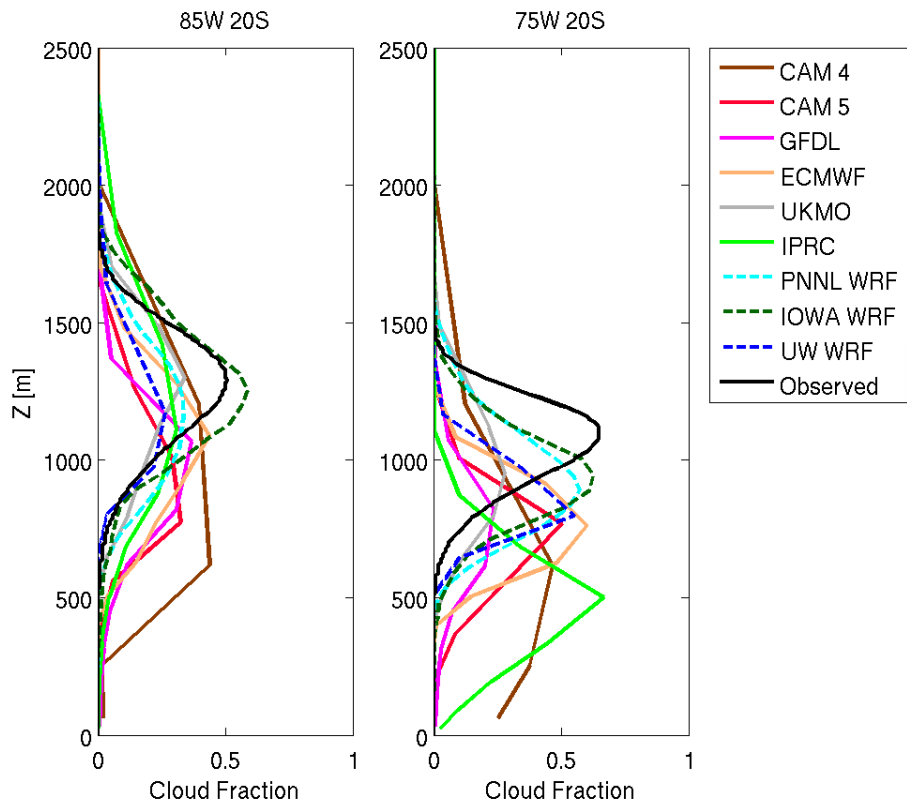
Fig. 5. Mean model cloud fraction at 85° W 20° S (left panel) and at 75° W 20° S (right panel). Also plotted is cloud fraction inferred from ship based measurements over nearby longitudes from Burleyson et al. (2013). See text for more details.
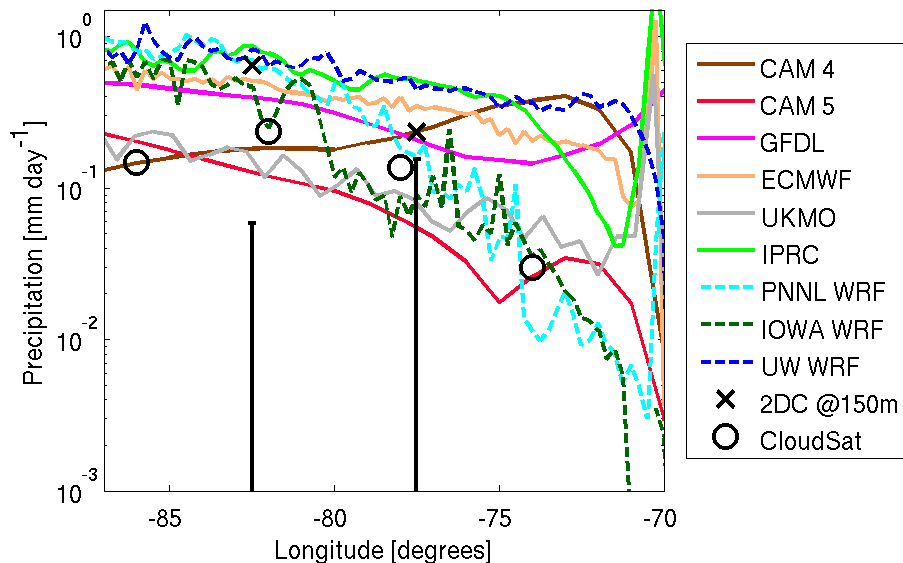
Fig. 6. Mean surface precipitation in mm day^{-1} along 20° S compared with leg-mean precipitation rate from C-130 estimates at 150 m using a 2D-C probe, and with CloudSat climatology for October–November 2007–2010. Error-bars show interquartile values for the 2D-C measurements. The 2D-C precipitation mean for 70–75° W is less than 0.001 mm day^{-1} and not shown.
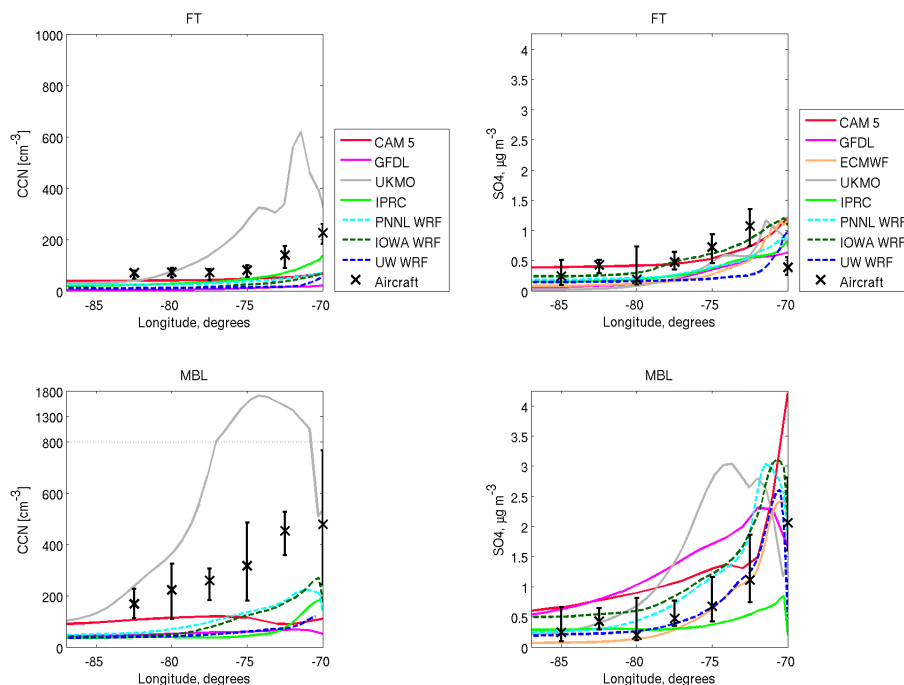
Fig. 7. CCN concentrations at 0.1 % supersaturation in cm^{-3} along 20° S are shown in the left panels. Free tropospheric (FT) mean (top left) and concentration at 150 m (lower left). C-130 nephelometer means are plotted with "x" symbols. Sulfate aerosol (SO$_4$) dry mass concentrations in µg m^{-3} of diameter range 0.05 µm – 0.5 µm measured with AMS (C-130 and BAe-146) are compared with model dry mass concentration along 20° S (see Allen et al., 2011) in the right panels for the FT (top right panel) and MBL mean (bottom right panel) The lower left plot is linearly rescaled at the top of the plot. The lower right panel is modified from a figure in Mechoso et al. (2013) to add aircraft sampling variability.

Title Page

Abstract | Introduction

Conclusions | References

Tables | Figures

|◄ | ►|

◄ | ►

Back | Close

Full Screen / Esc

Printer-friendly Version

Interactive Discussion
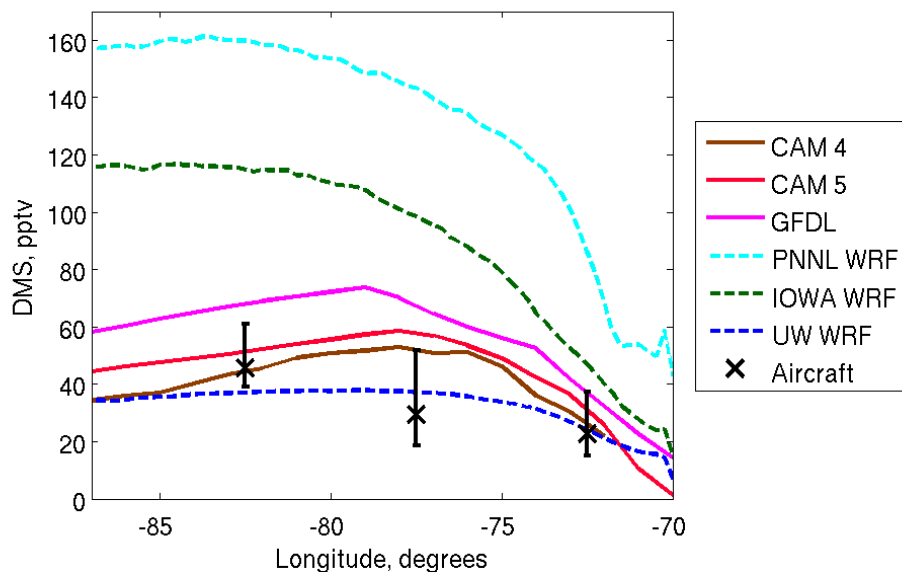
Fig. 8. MBL-mean DMS concentrations in pptv along 20° S for some models with C-130 observed means.
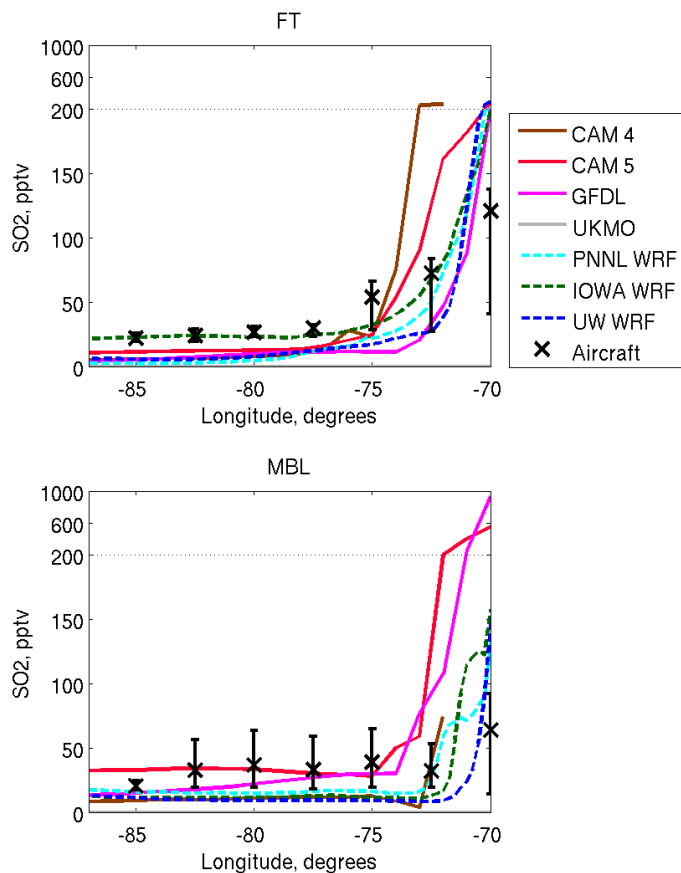
Fig. 9. Mean modeled SO_2 (gas) concentration along 20° S in pptv and C-130 aircraft means. The top sections of the both panels are rescaled.

Title Page

Abstract | Introduction

Conclusions | References

Tables | Figures

|◄ | ►|

◄ | ►

Back | Close

Full Screen / Esc

Printer-friendly Version

Interactive Discussion

Modeling of clouds
and aerosols during
VOCALS
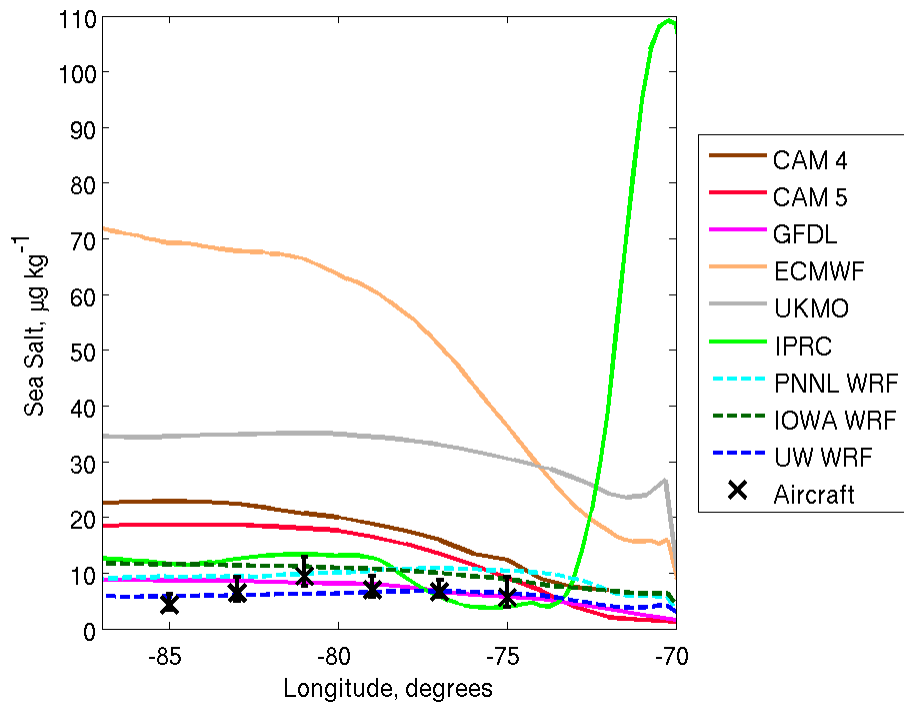
M. C. Wyant et al.

Fig. 10. Mean aerosol SSA dry mixing ratio along 20° S (µg kg^{-1}) compared with C-130 particle counter and Giant Nuclei Impactor measurements from Blot et al. (2013).
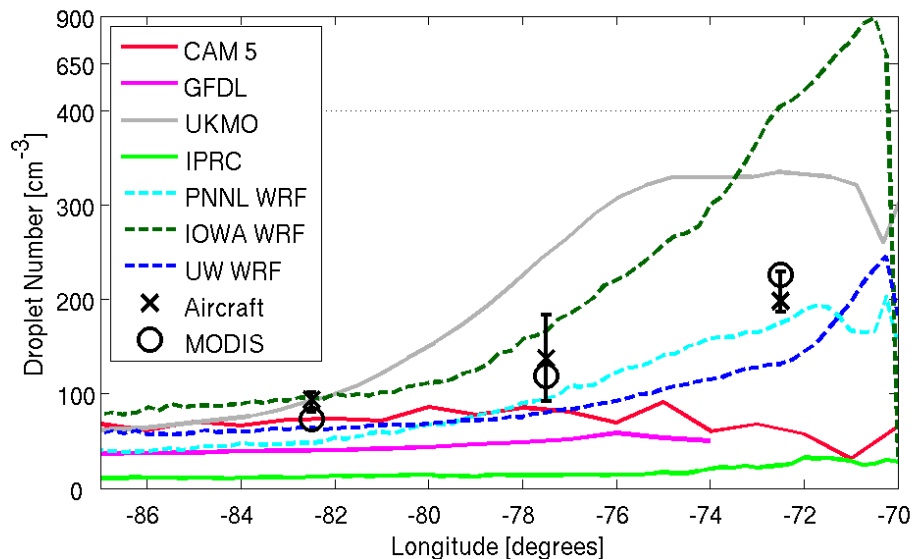
Fig. 11. Mean cloud droplet number concentration, N_d, in cm^{-3} along 20° S compared with mean C-130 measurements using a PMS cloud droplet probe and FSSP and also with MODIS estimates. This figure is modified from Mechoso et al. (2013) to add aircraft sampling variability and MODIS data. The top section of the plot is rescaled.

Modeling of clouds and aerosols during VOCALS

M. C. Wyant et al.
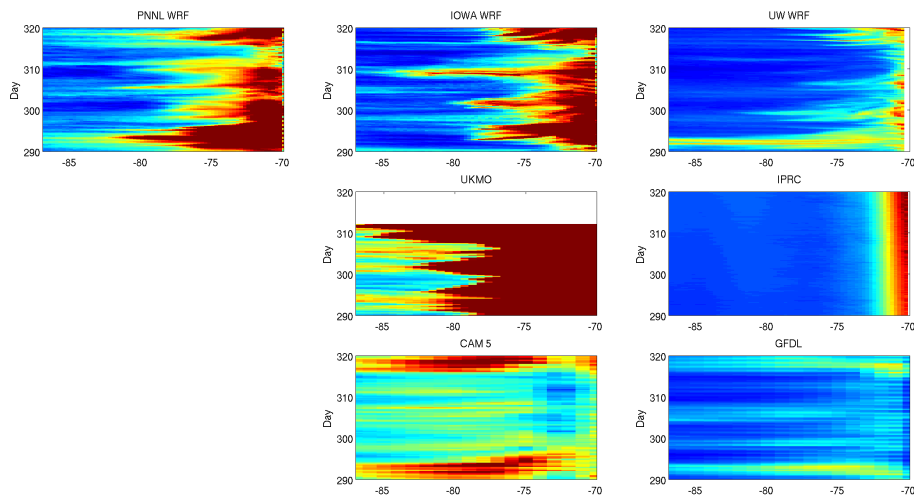
Fig. 12. Hovmöller diagrams of CCN at 0.1 % supersaturation at 150 m height along 20° S. CCN concentrations are given in cm^{-3}.
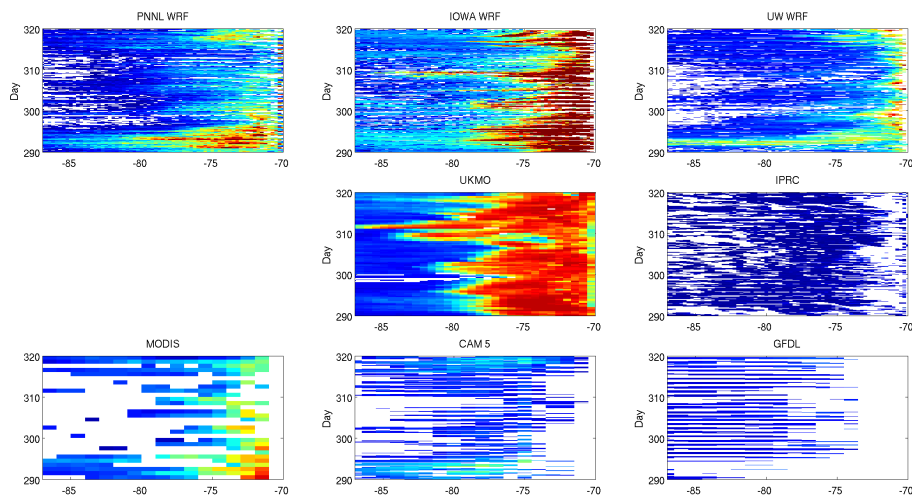
Fig. 13. Hovmöller diagrams of models' mean cloud droplet concentration, N_d, in cm^{-3} along 20° S. Daily mean MODIS estimates from Bretherton et al. (2010) are shown in the lower left.
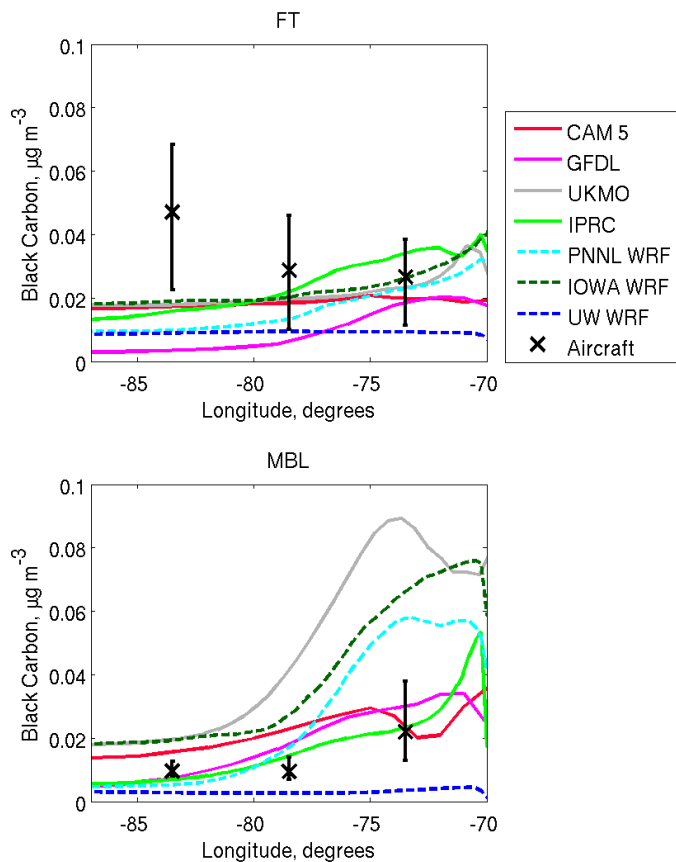
Fig. 14. Total modeled black carbon aerosol mass concentration ($\mu g\,m^{-3}$) along 20° S compared with C-130 single-particle soot photometer measurements (diameters 0.087–0.4 μm).

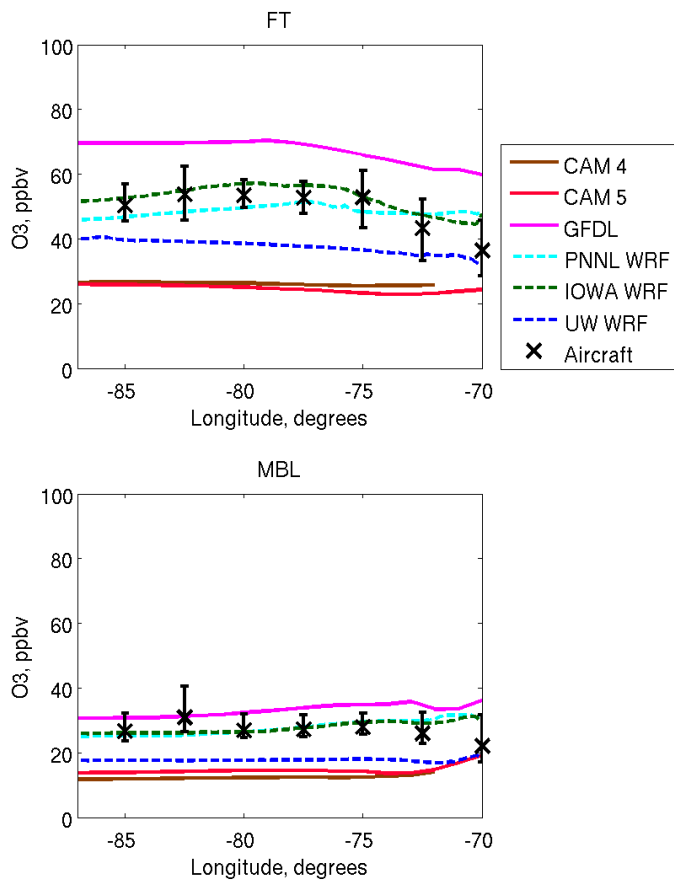**Fig. 15.** Ozone concentration (ppbv) compared along 20° S with C-130 and BAe-146 aircraft observations.

Title Page

Abstract | Introduction

Conclusions | References

Tables | Figures

|◀ | ▶|

◀ | ▶

Back | Close

Full Screen / Esc

Printer-friendly Version

Interactive Discussion